NTNU – Trondheim
Norwegian University of
Science and Technology

Comparison of Dry Gas Seasonal Storage with CO2 Storage and Re-Use Potential

Marie Killerud

Petroleum Geoscience and Engineering
Submission date: July 2013
Supervisor: Philip Ringrose, IPT

Norwegian University of Science and Technology
Department of Petroleum Engineering and Applied Geophysics

NORWEGAN UNIVERSITY OF SCIENCE AND TECHNOLOGY

Abstract

Faculty of Engineering Science and Technology
Department of Petroleum Engineering and Applied Geophysics

Master Thesis

Comparison of Dry Gas Seasonal Storage with CO_2 Storage and Re-Use Potential

by Marie KILLERUD

To make large-scale CO_2 storage economic, many groups have proposed using CO_2 in EOR projects to create value for CO_2 storage. However, CO_2 EOR projects generally require a large and variable supply of CO_2 and consequently may require temporary storage of CO_2 in geological formations. In order to store CO_2 at offshore sites as a source for CO_2 EOR projects, the CO_2 needs to be extracted from a storage site to a certain extent. Alternatively, CO_2 EOR projects may be developed alongside saline aquifer CO_2 storage with only some of the CO_2 being used for EOR. The idea of temporary storage of CO_2 may therefore be a key part of the solution for today's climate challenge regarding CO_2 emissions. Seasonal storage of dry methane gas is a well-established technique, and based on this project, it can also work for CO_2. This project examines the effectiveness of geological storage and re-use of CO_2 compared to seasonal dry gas storage. The controls on injection and production of CO_2 from an ideal storage geological site is estimated.

Sammendrag

Sesongbasert lagring av metangass er en teknikk som er mye brukt, men kan denne teknikken brukes med CO_2? Hvis man får lagring av CO_2 til å bli økonomisk, samtidig som dette tiltaket er med på å forhindre utslipp av CO_2, vil det være av nytteverdi for samfunnet med tanke på klimautfordringer. Ideen er å lagre CO_2 midlertidig, slik at gassen blir tilgjengelig for bruk i prosjekter for økt olje- og gassutvinning i fremtiden.

Hovedtema for denne oppgaven har vært sammenligning av sesongbasert lagring av metan kontra CO_2. Ved hjelp av sensitivitetsanalyser og simuleringer i Eclipse basert på en matematisk modell, ble det konkludert med at CO_2 kan lagres sesongbasert.

Resultatene viste at det var forskjeller mellom gassene, der spesielt fem parametere ble fokusert på; geometri, permeabilitet, oppløsning av CO_2 i vann, gjenværende metning av gass, og trykkstøtte fra underliggende akvifer. Både CO_2 og metan ble påvirket av gjenværende metning av gass i stor grad. I motsetning til metan, har CO_2 en stor evne til å løse seg i vann, noe som fører til at en større del av CO_2 blir gjenværende i reservoaret.

Hovedgrunnene til forskjellene mellom metan og CO_2 ligger i at metan er en mye mer kompressibel gass enn CO_2. Tetthetsforskjellene er store, der CO_2 sin tettheten i stor grad er trykkavhengig.

For å kunne ta i bruk teknikken om sesongbasert lagring av CO_2, bør en modell, slik som den i Collier sin artikkel brukt for metan, utledes på nytt for CO_2. Det bør derfor rettes et stort fokus på fanget gass, og da spesielt effekten av oppløst CO_2 i vann.

Acknowledgements

This diploma thesis presents the work completed in accordance with the course TGB4900 for The Norwegian University of Science and Technology (NTNU), at the Department of Petroleum Engineering and Applied Geophysics. It was written during the spring/summer 2013.

Special thanks goes to Dag Wessel-Berg at SINTEF, for giving me the start-up data file for use in Eclipse, for the time he spent on helping me building the numerical methods and simulation models, and for all the explanations and feedback he gave to me.

Moreover, I very much appreciate Philip Ringrose from Statoil ASA for making this thesis possible by being my supervisor, for providing reading material and for his guidance throughout the thesis, and for providing feedback. I would like to thank Bamshad Nazarian for help with Eclipse.

I would also thank my fellow students and friends for help and support during the semester.

Trondheim, July 2013

Marie Killerud

Contents

Abstract i

Sammendrag ii

Acknowledgements iii

List of Figures vii

List of Tables xi

Symbols xiii

1 Introduction 1

2 Literature Review 3
- 2.1 Development of underground storage reservoirs and basic concepts . 3
- 2.2 Development of aquifer storage reservoirs 4
- 2.3 Objective of engineering and design efforts 5
- 2.4 Temperature and pressure gradients in gas storage wells 7
- 2.5 Previous work and its usage for further research 7

3 Simple Model for Modeling Natural Gas Reservoirs -Based on the Collier 1981 SPE Paper 9
- 3.1 Goals with Calculation 9
- 3.2 Assumptions 9
  - 3.2.1 Derivations of Simple Governing Equations 9
  - 3.2.2 Numerical solution to Collier model 13
  - 3.2.3 An Implicit Method for Solving the Equations 14

4 Testing and Validating Against Published Data 17
- 4.1 Reservoir A 17
  - 4.1.1 Results from Excel 18
  - 4.1.2 Analysis of the Results 21
  - 4.1.3 Unit Issues -SI units 21

5 Evaluation of Controlling Parameters in the Collier Model 23
5.1 Sensitivity of Parameters in the Implicit Method 23
5.2 Observations from the Sensitivity Analysis 29

6 Eclipse Simulations 31
6.1 The Eclipse Simulator 31
6.2 Description of the Comparison between Collier and Eclipse 31
6.2.1 Simulation Result of Modelling Natural Gas Reservoir Based on Collier et al., 1981. 33
6.2.2 Rate R(t) 33
6.2.3 Cyclic Storage of CO_2 34
6.2.4 Deeper Storage of Methane 35
6.3 Sensitivity of methane storage versus CO_2 storage 38
6.3.1 Residual Trapping 38
6.3.2 Degree of Pressure Support 42
6.3.3 Geometry 45
6.3.4 Permeability 46
6.3.5 Dissolution 50
6.4 Summary of the application of the model in Eclipse 53

7 Discussion 55

8 Conclusion 59

A Calculations of the Gas-Water Contact 61

B Data File for Cyclic Storage of Methane 63

C Data File for Cyclic Storage of CO_2 77

Bibliography 93

List of Figures

2.1 General profile of an anticline used for cyclic storage of gas. Note the possible leakage paths through fault, wellbore and broken caprock. Also note that the gas-water contact may change due to different pressure support from the aquifer according to different permeability in the reservoir and aquifer, and different pressures from the wellbores. . . . 5

4.1 Picture taken from Collier et al., 1981. Plot of measured pressures, calculated pressures and production data versus time for Reservoir A. The rate function q(t) equals to the lower graph in the picture. . . 19
4.2 Recreated pressure curve with respect to time from the implicit model. 20
4.3 Recreated pressure curve with respect to time from the explicit model. 20
4.4 Comparison between the original pressure curve calculated in the Collier paper versus the recreated curves from the implicit and explicit model with respect to time. . . . 21

5.1 Sensitivity of the Schilthuis water drive constant with respect to different percentages of the original value of C^* from Reservoir A. . 24
5.2 Sensitivity of time step (Dt). Average pressure versus time is shown for dt= 0.168 and dt=0.084. . . . 25
5.3 Sensitivity of time step (Dt). Average pressure versus time is shown for dt=0.042 and dt= 0.084. . . . 25
5.4 Sensitivity of the gas entrapment factor with respect to its pressure, tested in Reservoir A. . . . 26
5.5 Sensitivity of how the volume rate of trapped gas, $\dot{V}_T$ respond to different values of the gas entrapment factor F_g. . . . 26
5.6 Sensitivity of the initial pressure with respect to different values tested in Reservoir A. . . . 27
5.7 Sensitivity of the initial gas in place with respect to its pressure, tested in Reservoir A. . . . 28
5.8 Comparision between the improved graph based on the implicit method and the graph from Collier's paper after changing the value of G_i and C^*. . . . 30

6.1 Base case geometric model from FloViz. . . . 32
6.2 Relative permeability of gas and water versus water saturation during 1 cycle. . . . 32

6.3 Cyclic storage of Methane from Collier et al., 1981. compared to the simulated model. Average pressure is shown during each cycle. Note that the first clearly spike appears after two years for the simulated model; the pressure response after one cycle is not represented. . . 33
6.4 Field reservoir pressure versus time for the base case cyclic storage of CO_2. 34
6.5 The base case cyclic storage graphs of methane versus CO_2. Methane and CO_2 shows different pressure curves, even when the geology for cyclic storage was the same. 35
6.6 The base case cyclic storage graphs of methane and CO_2 when it comes to different amounts of gas in place in the reservoir versus time. 36
6.7 Total compressibility of methane and CO_2 at 35°C. 36
6.8 Cyclic storage of methane showing the bottom hole pressures for injection and production with time. 37
6.9 Cyclic storage of CO_2 showing the bottom hole pressures for injection and production with time. 38
6.10 The general relative permebility of water and gas during 1 cycle without hysteresis. 39
6.11 Cyclic storage of methane with and without hysteresis. The average pressure with time is shown. 40
6.12 Cyclic storage of methane with and without hysteresis. Showing the differences in reservoir volume of gas in place with time. 41
6.13 Cyclic storage of CO_2 with and without the effect of hysteresis. The difference in reservoir volume of gas in place in shown with time for the two cases. 41
6.14 Volume rate of produed water with time. 42
6.15 Reservoir pressure versus time for cyclic storage of methane when the aquifer pressure support was taken into account. 43
6.16 Reservoir pressure versus time for cyclic storage of CO_2 when the aquifer pressure support was taken into account. 43
6.17 Volume of gas in place versus time for cyclic storage of methane based on aquifer pressure support. 44
6.18 Volume of gas in place versus time for cyclic storage of CO_2 based on aquifer pressure support. 44
6.19 Average reservoir pressure versus time for cyclic storage of both CO_2 and methane. 45
6.20 Reservoir pressure versus time for cyclic storage of both CO_2 and methane. 46
6.21 Reservoir volume of gas in place versus time during cyclic storage of methane. Two cases with different geometries are represented; an anticline geometry with depth of 100m (base case) and one of 50m. 46
6.22 Reservoir pressure versus time for cyclic storage of CO_2. 47
6.23 Reservoir pressure versus time for cyclic storage of methane. 47

6.24 Volume of gas in place versus time for cyclic storage of CO_2. . . . 48
6.25 Volume of gas in place versus time for cyclic storage of methane. . 48
6.26 Cyclic storage of CO_2. Bottom hole pressure graphs for injection of the two cases. 49
6.27 Cyclic storage of CO_2 showing the bottom hole pressures for production of the two cases. 49
6.28 Volume of free gas in place versus time for cyclic storage of CO_2 with and without dissolution effects. 50
6.29 Residual saturation of CO_2 after one cycle of injection and production. 51
6.30 Residual saturation of CO_2 after 9 cycles of injection and production. 51
6.31 Residual saturation of CO_2 after 4 years of cyclic storage for a realistic case, versus an ideal case. 52

7.1 Cyclic storage of CO_2 showing important factors. 55
7.2 Residual saturation of CO_2 after 4 years of cyclic storage for a realistic case, versus an ideal case. 57

A.1 Derivations of a gas volume using a rotational body with cylindrical coordinate system. 62
A.2 Derivations of the depth from the cap rock down to the gas-water contact. 62

List of Tables

4.1 Reservoir data of Reservoir A 19
4.2 Unit conversion from matric to SI 22

6.1 The different simulation cases 39
6.2 The different simulation cases and their most important observations. 53

Symbols

C	Generalized Schilthuis water drive constant	cu ft/yr/lbm mol or m^3/kPa/kmol
C^*	Schilthuis water drive constant	W cu ft/yr/psia or m^3/a/kPa
F_g	Gas entrapment factor	dimensionless
G	Instantaneous amount of gas in reservoir at time t=0	lbm mol or k mol
G_i	Initial amount of gas in place at time t=0	lbm mol or k mol
G_T	Cum. amount of trapped gas behind the water front at time t	lbm mol or k mol
G_P	Cum. amount of produced gas up to time t	lbm mol or k mol
p	Reservoir pressure	psia or kPa
p_i	Initial reservoir pressure	psia or kPa
$q_g(t)$	Rate of gas production	lbm mol/yr or k mol/a
$\mathbf{r}$	Position vector	ft or m
R	Universal gas constant	(psia-cu ft)/(lbm mol-°K) or (kPa.m^3)/(k mol·K)
t	Time	years
$dt, \triangle t$	Time step	years (or days)
T_i	Initial reservoir temperature	°K
v_i	Initial specific volume	cu ft/ lbm mol or m^3/kmol
V	Instantaneous reservoir volume	cu ft or m^3
V_i	Initial reservoir volume	cu ft or m^3
V_T	Volume of trapped gas	cu ft or m^3
W_e	Volume of water influx	cu ft or m^3
$\bar{\rho}$	Average gas density	lbm mol/cu ft or kmol(m^3)

ρ	Gas density	lbm mol/cu ft or kmol(m^3)
m	Time steps	year
j	Time steps	year
n, N	Counter	dimensionless
c	Constant	m^3/day^2
R(t)	General rate function	m^3/day
V_{por}	Pore volume	m^3
Q	Reservoir volume injected or produced	m^3
c_T	Compressibility	bar^{-1}
k	Permeability	mD

1. Introduction

Fossil fuel combustion supplies the major part of the energy for the industry, where coal is estimated to increase its supply in the future, resulting in increased CO_2 emissions [Haszeldine, 2009]. The importance of CO_2 storage is to prevent CO_2 emissions, which in turn will help to prevent global temperature rise. In order to make large-scale CO_2 storage economic, a solution where CO_2 can be stored temporarily may be desirable.

The science and technology behind carbon capture and storage is already partly developed [Poulsen, 2012]. It has been used in enhancing oil and gas recovery since 1960, and for geological storage since 1996. Today, a number of CCS demonstrations are ongoing around the world at various stages of development. The demonstrations span a large variety, both in geological environment, cost environment and site histories [Eiken et al., 2010]. To create value for CO_2 storage, many groups have proposed using CO_2 in EOR projects. A limitation may be the supply of CO_2, which depends on the available CO_2 at that time. A large and variable supply of CO_2 which consequently may require temporarily storage of CO_2 in geological formations would be desirable. Seasonal storage of dry methane gas has been practiced since 1915 due to the variable marked demand of energy. Significant growth started in 1950 where storage has been done in aquifers, depleted hydrocarbon reservoirs and salt cavities [Katz and Tek, 1981]. CO_2 have other properties that make the storage different comparing to methane. Several factors will affect the amount re-produced CO_2, among residual trapping of CO_2, CO_2 dissolution, CO_2 PVT properties, the geometry and permeability of aquifer, and the degree of aquifer pressure support.

To make seasonal storage of CO_2 possible, several issues need to be addressed. The technology and idea of carbon capture and storage, together with the technology for seasonal dry gas storage may be combined to develop a method for seasonal storage of CO_2. Both measurements and simulation tools can be used to evaluate how effective CO_2 can be stored and re-produced.

In this thesis, the focus will be on comparing dry gas seasonal storage with re-use potential from CO_2 storage sites. On basis of the review in this thesis, where the theory of seasonal gas storage are described, a solution where CO_2 can be stored temporarily may be desirable. CO_2 may then be extracted from the temporarily storage site when needed, e.g. during an EOR project, and then permanently stored later.

A simplified model for modelling natural gas reservoirs [Collier et al., 1981] is tested and validated. A simulation study made for optimal CO_2 storage with extraction will be made before returning back to the model for revising the version for modelling CO_2 storage with extraction.

2. Literature Review

2.1 Development of underground storage reservoirs and basic concepts

Underground gas storage have been practiced since 1915, and significant growth started in 1950 [Katz and Tek, 1981]. Storage of gas is done in aquifers, depleted hydrocarbon reservoirs, and salt cavities. Because of wide availability, depleted hydrocarbon reservoirs are the most common underground storage site [eia]. Enhanced oil recovery is sometimes part of the objective, but complications may occur due to liquids in the wellbore, possible enrichments of gas and condensate formation in the pipeline. It is also possible that gas goes into solution with crude oil, which decrease the amount available gas. Following this, aquifer storage is an alternative storage site for gas.

The concept of underground storage is a process that effectively balances a variable marked demand with a nearly constant supply of energy. It involves the cyclic pressurization and depressurization of the reservoir, and works as a warehouse for gas. The gas is generally stored in the summer months, and then supplies the marked for periods of high demand in the winter months. The storage unit often lies above an aquifer or residual oil leg, which may lead to some cyclic motion of the gas-liquid contact and gas zone. [Bietz et al., 1996], and [Collier et al., 1981].

Both a pseudo steady state equation and a classical unsteady state solution [Everdingen and Hurst, 1949] are methods used for characterizing the changing conditions in an aquifer. The unsteady state solution is valid for a variety of geometries, including infinite aquifers. The concept of underground storage consists of multiple variables, which often are mutually dependent. According to Duane J. W.

and Mich J. (1967), the variables are 1) potential cyclic capacity and peak-day rate market requirements, 2) number of wells, 3) compressor inlet line pressure, 4) overpressure, 5) average well open flow and back pressure slope, 6) casing size, and 7) gathering system designs.

2.2 Development of aquifer storage reservoirs

The most promising prospective sites for aquifer storage are pure water-bearing sands with anticline structures, see figure 2.1. To locate and characterise the structure, exploration wells are drilled and cores are evaluated to show the value of porosity, permeability and capillary pressure functions. Cores from the caprock are evaluated in the same manner including measurements for checking how much the caprock withstands. The pressure distribution as function of time is hard to predict, especially predicting the situation many years into the future after years of operation [Katz and Tek, 1981]. It is important to pay attention to the water influx and efflux that affect the aquifer during gas storage, as a certain amount of injected gas may never be extracted from the aquifer. Like in depleted reservoirs, gas production stops when there is no pressure differential left between the wellhead and the reservoir to push the gas out of the reservoir. In addition, an aquifer contains a larger volume of gas, called base gas, which must remain in the aquifer to provide the required pressure needed to extract the remaining gas [eia].

In order to maximise the re-production of gas from a financial point of view, a high production of the base gas is desired. When the water drive is substantial, the problem arises where water seals off residual gas at its prevailing pressure. To produce as much as possible, it is suggested to produce as rapidly as possible ahead of the invading waterfront [Katz and Tek, 1981]. Cautious monitoring of injected and withdrawal performance is needed in order to control the reservoir pressures when it comes to changes in water influx$'$ and efflux$'$ together with injection and production performances.

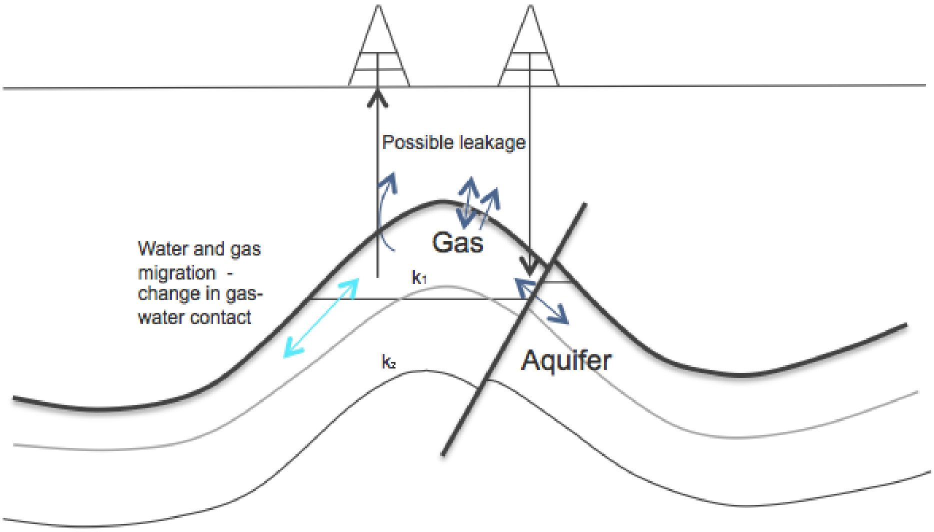

FIGURE 2.1: General profile of an anticline used for cyclic storage of gas. Note the possible leakage paths through fault, wellbore and broken caprock. Also note that the gas-water contact may change due to different pressure support from the aquifer according to different permeability in the reservoir and aquifer, and different pressures from the wellbores.

2.3 Objective of engineering and design efforts

According to Katz et al (1981), there are three main objectives in designing and operating storage gas reservoirs. The first one is termed verification of inventory, and addresses the storage capacity for gas as a function of pressure. The second is called retention against migration, and concerns monitoring whether the gas is retained, or if some losses are occurring. The last objective is called assurance of deliverability, and addresses the ability to develop and maintain a specified gas deliverability rate.

The movement of gas beyond the original gas/water contact has been observed in field with an active water drive during cyclic injection and production of gas. Close attention should be given to verification of gas inventories in order to maintain the storage-field performance and because of the cost considerations. In order to address the gas loss in water driven aquifers, a year-to-year change in the cumulative volume of gas withdrawal when the deliverability declines to a given volume may be observed [Mayfield, 1981]. Computer simulations is another helpful tool when it comes to inventory verification where production-pressure behaviour of a storage reservoir is needed [Katz et al., 1963].

Possible losses from the connected gas bubble body are: through imperfect cementing at casing shoe, leakage in cementing tool or casing joints, separation of the gas from the bubble through a saddle point when gas is displacing water, or in aquifers where gas loss take place vertically through imperfections in caprock due to low local pressure areas. Location wells are drilled to permit monitoring of the gas when the gas-bubble grows in size. If the deeper aquifer zone has higher permeability, the gas may migrate deeper than intended [Katz and Tek, 1981]. Often more than one reservoir compartment may be involved in a gas storage system. If two reservoirs are located close to each other on the same horizontal level, and unequal pressures exist between the reservoirs, this may result in transfer of gas from one reservoir to the other. The flow rates between them are of interest. Therefore, when a new aquifer is to be selected for gas storage, a survey of the nearby area needs to be done [Katz and Tek, 1981].

It is important to predict the field flow at several stages of a gas storage cycle. This can be done by monitoring the wells, study gas inventory, reservoir pressure measurements and deliverability data. The case of a heterogeneous reservoir that results in a decrease in pressure during high withdrawal rates of the gas may results in less predictable storage performance. Interference of water reaching the wellbore is another problem that may occur. The water will reduce the relative permeability to gas, and also reduce the efficiency of the bottom hole drawdown pressure due to gas flow because of increased fluid density in the well. This problem will subside with gas-bubble growth. One example taken from Michigan Stray sand reservoirs had deliverability that declined 4.5% each year due to oil residues, shale sloughing, salt precipitation and fines. It is possible to increase the percent by injecting different chemicals [Katz and Tek, 1981].

One technique used for determining the optimal design is a graphical technique called the field design optimization graph. The technique enables one to easily scan the spectrum of potential field operations against total development costs [Duane and Mich, 1967]. It is more challenging to determine the optimal design in aquifers with water drive. Some of the gas injected proceeds away from the main gas body, sometimes for large distances, and may become out of control [Katz et al., 1963]. To analyse the repetitive cycles, and improve the pressure volume calculations to ascertain gas inventory, a concept called pound x day is frequently used. It is based on the pseudo steady state of water movement caused by the complex unsteady state conditions due to changing conditions in the aquifer storage [Katz and Shah, 1984].

2.4 Temperature and pressure gradients in gas storage wells

The temperature in the well during production differs from that during injection. When gas, which is not heated fully, enters the porous storage rock, the rock will cool down rapidly. The area will have subgeothermal temperature until significant withdrawal occurs. During withdrawal, the wellbore reach faster the equilibrium geothermal gradient than the storage rock. Alternate cooling and heating of the casing and thereby cement, may cause deleterious effects on the cement bond, resulting in a need for recementation [Katz and Tek, 1981].

2.5 Previous work and its usage for further research

In the sections above, a review has been presented, describing general principles about theory and methods used for cycling gas storage. Could the same principles apply to CO_2 storage, or are there different factors? These study will investigate these aspects, and finally conclude with a model for CO_2 storage including the applicable principles.

3. Simple Model for Modeling Natural Gas Reservoirs -Based on the Collier 1981 SPE Paper

3.1 Goals with Calculation

In order to make a model for CO_2 seasonal storage, a model based on gas storage was developed as a starting point for further research. The simplified model of Collier (1981) was selected for this purpose, where the goal was to get the new model to match the results from the Collier′s model. The model was made to test the production of natural gas with water encroachment and gas entrapment [Collier et al., 1981].

3.2 Assumptions

3.2.1 Derivations of Simple Governing Equations

The Collier model comprises a material and volumetric balance relation together with the Schilthuis water drive model, with gas entrapment mechanism included. The rate of gas entrapment is assumed to be proportional to the volumetric rate of water influx. The model is zero-dimensional, which means it does not deal with the structures of the model. The distributed variables do not vary with position, but are replaced by single effective quantities, like an average value of the variable. The equations below are examples of how to utilize a zero-dimensional model.

To calculate the physical properties of fluids in the reservoir, an equation of state is developed. The ideal gas law is employed in order to get expressions for molar gas in reservoir, and volume of gas in reservoir. The classical ideal gas low may be written:

$$pV = GRT \tag{3.1}$$

where T is the temperature of the reservoir. R is the universal gas constant, p is the average pressure, V is the gas volume, and G is the molar amount of gas in the reservoir.

The following variables are introduced:

p_i, T_i, G_i and V_i: initial pressure, temperature, mole gas in reservoir, volume of gas in reservoir.

p, G, V: average volume pressure, mole gas (free) in reservoir, volume of free gas.

W_e: volume of water influx.

G_T and V_T: trapped mole gas in reservoir and trapped volume of gas in reservoir.

F_g: gas entrapment factor.

After Schilthuis the volumetric influx of water from the surrounding aquifer is given by:

$$\dot{W}_e = C^*(p - p_i) \tag{3.2}$$

where, $[C^*] = m^3 s^{-1} bar^{-1}$ is a constant.

Assume a reservoir with a water-gas contact zone to an underlying aquifer. The water in the aquifer moves dynamically, and the volume rate of water influx ($\dot{W}_e$) flows into the reservoir when the average pressure in the reservoir has changed from the initial pressure. The initial pressure value is assumed to be similar to the pressure in the aquifer. The water drive constant (C^*) together with the pressure difference between the reservoir and aquifer tell how big the volume rate of water influx will be. It is assumed that the water at the gas-water contact traps a fraction of the gas. F_g is the gas entrapment factor, and together with the volume rate of water influx, the volume rate trapped gas $\dot{V}_T$ is then:

$$\dot{V}_T = F_g \dot{W}_e \tag{3.3}$$

since $V_T = W_e = 0$ at $t = 0$.

The molar trapped gas rate $\dot{G}_T$ is then

$$\dot{G}_T = \rho \dot{V}_T \tag{3.4}$$

where ρ is molar density. Note that when the pressure increases, ρ increases, trapping more mole gas per trapped unit of volume.

One assumes the ideal gas law for trapped gas to be:

$$\boxed{pV_T = G_T R T_i.} \tag{3.5}$$

Consequently from 3.2, 3.3, 3.4, and 3.1,

$$\dot{G}_T = \frac{C^* F_g}{RT_i} p(p_i - p). \tag{3.6}$$

Equation 3.6 gives the molar trapping rate as function of pressure. If $q_g(t)$ is the molar production rate, we consequently have

$$\dot{G} = -q_g(t) - \dot{G}_T. \tag{3.7}$$

Then, using 3.6 one obtains

$$\boxed{\dot{G} = -q_g(t) - \frac{C^* F_g}{RT_i} p(p_i - p).} \tag{3.8}$$

This equation is giving the molar rate of charge of free gas in the reservoir. Equation 3.8 is the mass balance equation.

We also need volume conservation in order to have a consistent set of equations for obtaining the average pressure $p(t)$ when $q(t)$ and initial values are given.

Since V + V_T + W_e is constant (since reservoir is assumed incompressible), $\dot{V} + \dot{V}_T + \dot{W}_e = 0$ express the volume conservation. Equations 3.2 and 3.3 gives:

$$\dot{V} + F_g C^*(p_i - p) + C^*(p_i - p) = 0$$

$$\Longleftrightarrow$$

$$\boxed{\dot{V} = -(1 + F_g)C^*(p_i - p).} \tag{3.9}$$

To conclude that the Collier model is a coupled system of non-linear ordering equations

$$\boxed{\dot{V} = -(1 + F_g)C^*(p_i - p)} \tag{3.9}$$

and

$$\boxed{\dot{G} = -q_g(t) - \frac{C^* F_g}{RT_i} p(p_i - p)} \tag{3.8}$$

with initial conditions:
$V(0) = V_i$
$G(0) = G_i$,
and when $q_g(t)$ is a given function, one gets $\dot{p}$ with use of the ideal gas law 3.1:

$$pV = GRT$$

$$G = \frac{pV}{RT}$$

Then, one derives G:

$$\dot{G} = \frac{(\dot{p}V + p\dot{V})}{RT_i}$$

and insert equation 3.9

$$\dot{G} = \frac{(\dot{p}V + p(-(1+F_g)C^*(p_i - p)))}{RT_i}. \tag{3.10}$$

If one inserts equation 3.10, into equation 3.8, one gets

$$\dot{p} = -\frac{p_i V_i}{G_i}\frac{q_g}{V} + \frac{C^*(p_i - p)p}{V}. \tag{3.11}$$

The functions are summarized as below:

$$\boxed{\dot{V} = -(1+F_g)C^*(p_i - p)} \tag{3.9}$$

$$\boxed{\dot{p} = -\frac{p_i V_i}{G_i}\frac{q_g}{V} + \frac{C^*(p_i - p)p}{V}.} \tag{3.12}$$

3.2.2 Numerical solution to Collier model

Two different numerical methods are used for solving 3.9 and 3.12 , one explicit forward Euler method is considered, and one implicit. First the forward Euler method is considered. Writing 3.9 and 3.12 in vector notation gives:

$$\begin{bmatrix} V \\ p \end{bmatrix}' = \begin{bmatrix} -C^*(1+F_g)(p_i - p) \\ -\frac{p_i V_i}{G_i}\frac{q_g(t)}{V} + \frac{C^*(p_i - p)p}{V} \end{bmatrix} \tag{3.13}$$

The system of equations can be expressed as

$$\begin{bmatrix} -C^*(1+F_g)(p_i - p) \\ -\frac{p_i V_i}{G_i}\frac{q_g(t)}{V} + \frac{C^*(p_i - p)p}{V} \end{bmatrix} = \vec{y}' = \vec{f}(\vec{y}, t), \tag{3.14}$$

with

$$\vec{y}(0) = \begin{bmatrix} V_i \\ p_i \end{bmatrix},$$

and

$$\vec{f}(\vec{y},t) = \vec{f}(p,V,t)$$

y_0 is given by the initial data. In the explicit method the quantities on the right hand of the equations are calculated from the previous step

$$\vec{y}_{n+1} = \vec{y}_n + \triangle t \cdot \vec{f}(\vec{y_n}, t_n)$$

The resulting equations, which are coupled on each other, are as follows:

$$\boxed{V_{n+1} = V_n + \triangle t(-C^*(1+F_g)(p_i - p_n))} \tag{3.15}$$

$$\boxed{p_{n+1} = p_n + \triangle t(-\frac{p_i V_i}{G_i V_n} \cdot \frac{(q_n + Q_{n+1})}{2} + \frac{C^*(p_i - p_n)p_n}{V_n})} \tag{3.16}$$

The values ${\{p_k\}^N}_{k=1}$ and ${\{V_k\}^N}_{k=1}$ were generated using an Excel spreadsheet.

3.2.3 An Implicit Method for Solving the Equations

The mass and volume conservation laws, together with the ideal gas law,

$$pV = GRT_i \tag{3.17}$$

gives the equation we want. Equation 3.6 gives:

$$G = G_i - \int\limits_0^t q_g(\tau)d\tau - \frac{C^* F_g}{RT_i}\int\limits_0^t p(\tau)(p_i - p(\tau))d\tau. \tag{3.18}$$

Equation 3.7 gives

$$V = V_i - (1+F_g)C^*\int\limits_0^t (p_i - p(\tau))d\tau. \tag{3.19}$$

These two equations inserted into the equation 3.17 gives:

$$p(V_i-(1+F_g)C^*\int\limits_0^t(p_i-p(\tau))d\tau=RT_i(G_i-\int\limits_0^t q_g(\tau)d\tau-\frac{C^*F_g}{RT_i}\int\limits_0^t p(\tau)(p_i-p(\tau))d\tau. \tag{3.20}$$

This equation can be written on another form,

$$\frac{\frac{G_iRT_i}{p_i}-(1+F_g)C^*\int\limits_0^t(p_i-p(\tau))d\tau}{RT_i}=G_i-\int\limits_0^t q_g(\tau)d\tau-\frac{C^*F_g}{RT_i}\int\limits_0^t p(\tau)(p_i-p(\tau))d\tau \tag{3.21}$$

which is the same equation as given in (14) Collier on discrete form.

The equation for p is an integral equation that is equivalent to the system of differential equations 3.13 described above, and equivalent to the system (13) of differential equations in Collier's paper.

To solve 3.21 one chooses time steps, and 3.21 in discrete form. To do this, define:

$$Q_k=\sum_{j=1}^k(q_g)_j\bigtriangleup t_j \tag{3.22}$$

$$A_k=\sum_{j=1}^k(p_i-p_j)\bigtriangleup t_j \tag{3.23}$$

$$B_k=\sum_{j=1}^k(p_i-p_j)p_j\bigtriangleup t_j \tag{3.24}$$

Then, (14) is the discrete form of

$$\begin{aligned}&\frac{p_m[v_iG_i-(1+F_g)C^*(A_{m-1}+(p_i-p_m)p_m)\bigtriangleup t_m]}{RT_i}\\&=G_i-Q_m-\frac{C^*F_g}{RT_i}(B_{m-a}+((p_i-p_m)p_m\bigtriangleup t_m))\end{aligned} \tag{3.25}$$

$$\Longleftrightarrow$$

$$\boxed{\begin{aligned}(C^* \triangle t_m)p_m^2 + (v_i G_i - (1+F_g)C^* A_{m-1} - p_i C^* \triangle t_m)p_m \\ +(Q_m RT_i + F_g C^* B_{m-1} - RT_i G_i) = 0)\end{aligned}} \tag{3.26}$$

where

$$C^* = G_i C \tag{3.27}$$

and

$$v_i = \frac{RT_i}{p_i}. \tag{3.28}$$

Thus, (14) is really a 2.degree equation for p_m when $p_0 = p_i, p_1, p_2, .., p_{m-1}, \triangle t_1,..,\triangle t_m$, and $(q_t)_1, .., (q_g)_m$

This method for solving the equations is implicit, as opposed to the previous explicit numerical method that is used solving 3.13.

The final second degree equation (3.26) has been implemented in Excel.

4. Testing and Validating Against Published Data

Now that the necessary equations and solutions for Collier model has been described. This section will show how the models are built, and how to use them. The working flow is as follows:

1. Find a suitable case, which agree with the assumptions, described in chapter 3.2.
2. Find the inputs: G_i, V_i, C, F_g p_i, T_i, $q(t)$
3. Find the number of time increments needed.
4. Do calculations in Excel based on the explicit method, which again is based on the simple method in the Collier paper [1981], and on the implicit method.
5. Analyse the results.

4.1 Reservoir A

The working equations and the assumtions for the simple model have been described in the previous chapter. An example of this simple method is presented in this chapter based on Reservoir A given in Collier [Collier et al., 1981]. The field is an old depleted gas reservoir converted to gas storage operations [Katz et al., 1963]. Before the field was converted to storage operations, it was shut in for several years, allowing water to encroach the depleted areas of the field successively. This resulted in a decrease in the original reserves, which are used as a initial condition of storage volume operations.

Relevant Field Data from Reservoir A

The table below show some of the characteristics of Reservoir A. The input values used are then:

$G_i = 3.17x10^{10}$ mole
$V_i = 2.83x10^7\ m^3$
$C = 2.5x10^{-2}\ m^3/kPa/year/mole$
$F_g = 0.003$
$p_i = 30.05$ bar
$T_i = 32$ ° C
$q(t) =$ function from picture

The production rate is taken manually from the instantaneous production graph in figure 4.1. The Values of F_g and C and G_i are calculated values taken from the Collier paper. The value of V_i equals the new reserve volume obtained in the reservoir before storage of gas. The temperature and initial pressure are taken from table 4.1.

Selection of the Time Increments
Number of time increments is set to be 50. This equals 4.2 years of production and injection of Reservoir A.

4.1.1 Results from Excel

The results from the implicit method is shown in figure 4.2, while the results from the explicit method is shown in figure 4.3. The results are shown in SI-units.

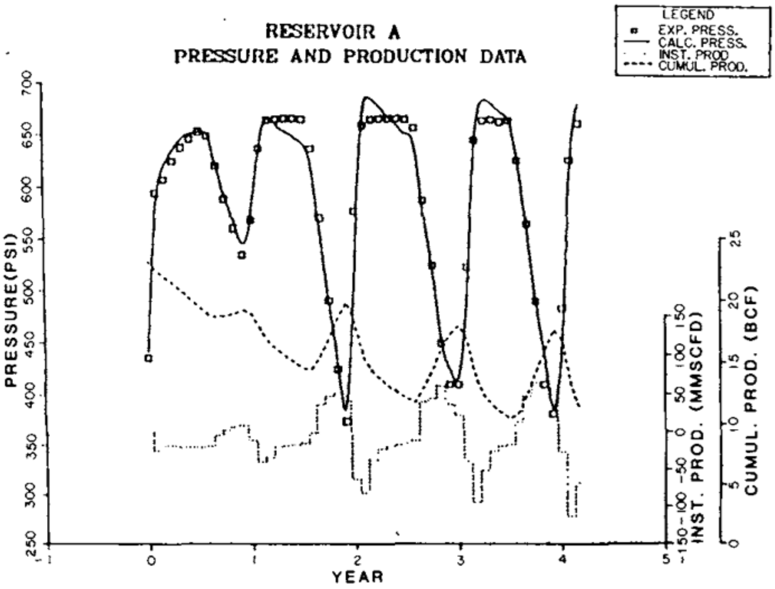

FIGURE 4.1: Picture taken from Collier et al., 1981. Plot of measured pressures, calculated pressures and production data versus time for Reservoir A. The rate function q(t) equals to the lower graph in the picture.

TABLE 4.1: Reservoir data of Reservoir A

Storage Reservoir A, Reservoir Data	
Aquifer	**Description/Value**
Rock Characteristics	
Formation	Sandstone and Limestone
Depth to top of aquifer	416m
Average net thickness	3.05m
Average porosity	30%
Average permeability	500 md
Fluid Characteristics	
Liquid viscosity	$1x10^{-3}$ Pa.s (assumed)
Compressibility of liquid and formation	$1,0152639x10^{-6}kPa^{-1}$
Gas Reservoir	
Rock Characteristics	
Formation	Sandstone
Structure	Anticlinale
Average reservoir thicness	3.05m
Field reserves	$2.83x10^{7}$ m^{3}
Fluid characteristics	
Reservoir temperature	32°C

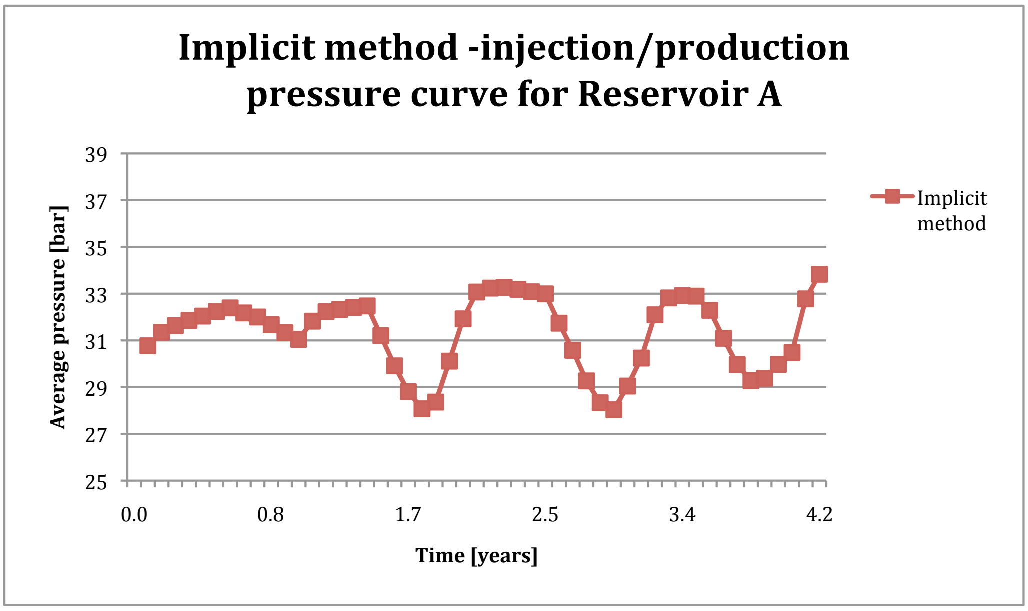

FIGURE 4.2: Recreated pressure curve with respect to time from the implicit model.

It can clearly be seen that both the figures shows the right trend for injection and production of gas. The graphs do not extend enough, they vary between 29 bars and 37 bar.

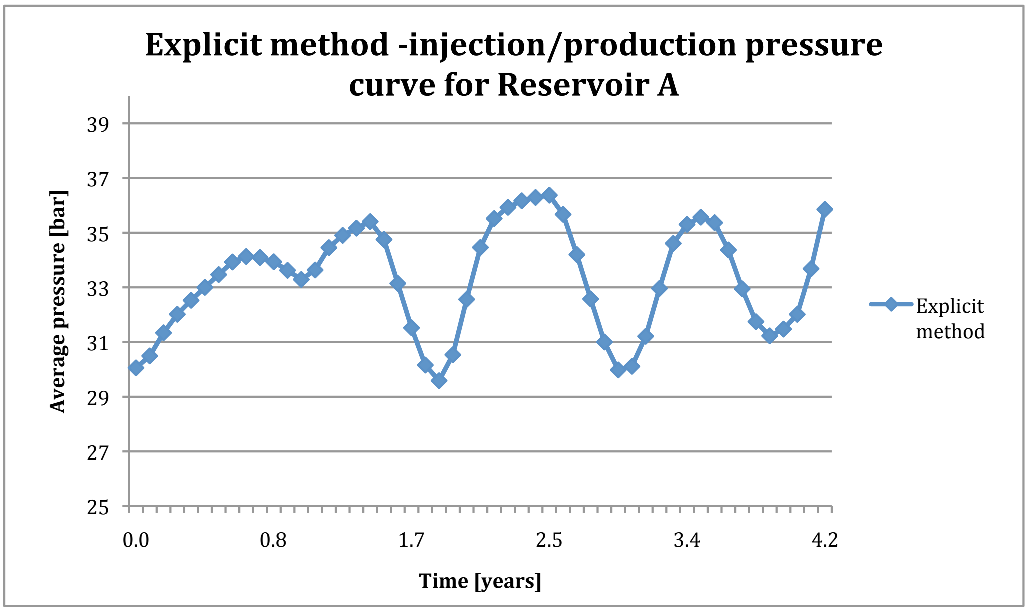

FIGURE 4.3: Recreated pressure curve with respect to time from the explicit model.

4.1.2 Analysis of the Results

Too easier see how similar the two methods and the Collier model are, they were plotted in the same plot to be compared to each other. Figure 4.4 shows how similar the two recreated methods are. Compared to the original model from Collier's paper, the implicit and explicit methods do not match. The trend is almost the same, but the average pressure is more pronounced in Collier's paper.

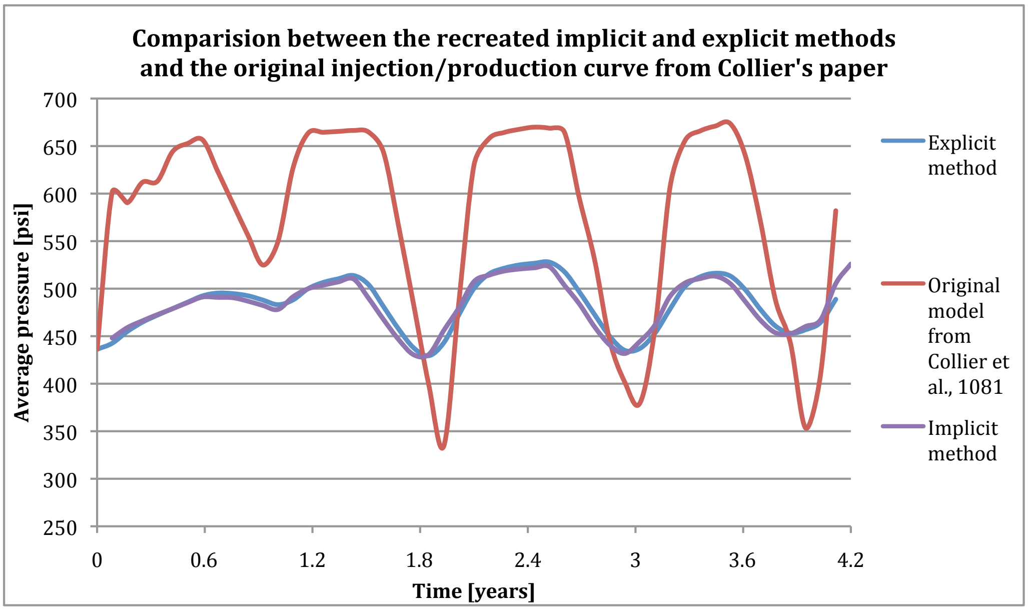

FIGURE 4.4: Comparison between the original pressure curve calculated in the Collier paper versus the recreated curves from the implicit and explicit model with respect to time.

There are large deviations between the two recreated methods, and the Collier model. From the author′ point of view, it was difficult to work with Collier′ paper because the way he prepared his model was unclear. The model and input data used in this project are the same as in the Collier model. Because two numerical systems were made in order to match the Collier model, and both gave the same results, it supports that the numerical systems are correct. It is therefore questioned if the Collier model is correct? In the next chapter, tuning to match the Collier model has been done.

4.1.3 Unit Issues -SI units

Table 4.2 below; shows the conversion from metric to SI units. Throughout the thesis, the units will be in SI units, except from when the results are compared with the original results in Colliers's paper.

TABLE 4.2: Unit conversion from matric to SI

SI Metric Conversion Factors		
Parameters	**Metric**	**SI**
Temperature	°F $\frac{(°F-32)}{1.8}$	=°C
Temperature	°F $\frac{(°F+459.67)}{1.8}$	=°K
Amount of gas	lbm mol x $4.535924x10^{-1}$	=kmol
Volume	ft^3 x $2.831685x10^{-2}$	$= m^3$
Volume	scf x $2.863640x10^{-2}$	= std m^3
Pressure	psi x $6.89x10^{-2}$	= bar
Schiltuis water drive constants (C)	$\frac{ft^3}{y \cdot psi \cdot lbmmol}$ x $9.0606624x10^{-1}$	$= \frac{m^3}{y \cdot bar \cdot kmol}$
Schiltuis water drive constants (C^*)	$\frac{ft^3}{y \cdot psi}$ x $2.83x10^{-2}$	$= \frac{m^3}{y \cdot bar}$
Rate	MMSCFD x $1.0333150x10^7$	$= \frac{m^3}{y}$
Universal gas constant	$\frac{J}{mol \cdot K}$ x $1x10^{-5}$	$=\frac{m^3 \cdot bar}{mol \cdot K}$

In the explicit method, the production/injection rate was transformed from cubic meters per year to mole per year by multiplying with the standard molar density of the gas in the reservoir:

$$\frac{m^3}{yr} \text{ x } 39.39 \; \frac{mole}{m^3} = \frac{mole}{yr}$$

The unit for the time steps is in years, where each time steps are divided into months.

5. Evaluation of Controlling Parameters in the Collier Model

In order to get a good model for storage of gas, sensitivity testing of each parameter has been done. In chapter 1 , a method for modelling natural gas reservoirs have been derived using an implicit method. Both the explicit and implicit method gave fairly similar results, which supports the numerical methods. The sensitivity analysis in this chapter is therefore chosen to be done on the implicit method. The sensitivity analysis allows us to know how good the method will work for different cases. Since every case of gas storage is different, the method needs to be valid for a range of different scenarios.

In the following, the implicit method for solving the Collier model has been used. All cases for the Collier model uses the Sm^3/day injection/production rate.

5.1 Sensitivity of Parameters in the Implicit Method

Schilthuis Water Drive Constant:
The pressure has been calculated for different values of the Schilthuis water drive constant (C^*). The range of values spans from 10% of the original C^* to an increase of 300%. Figure 5.1 shows that for decreased values of C^*, the pressure function increase for every cycle. For increased values of C^*, the pressure function decrease and the cycles get less pronounced. This observation shows that it takes more pressure to inject and produce the gas when the water in the formation does not flow as easily. In order to avoid high, and especially increasingly higher pressure for each cycle, the value of C^* should not be too low in a project of cyclic storage of gas.

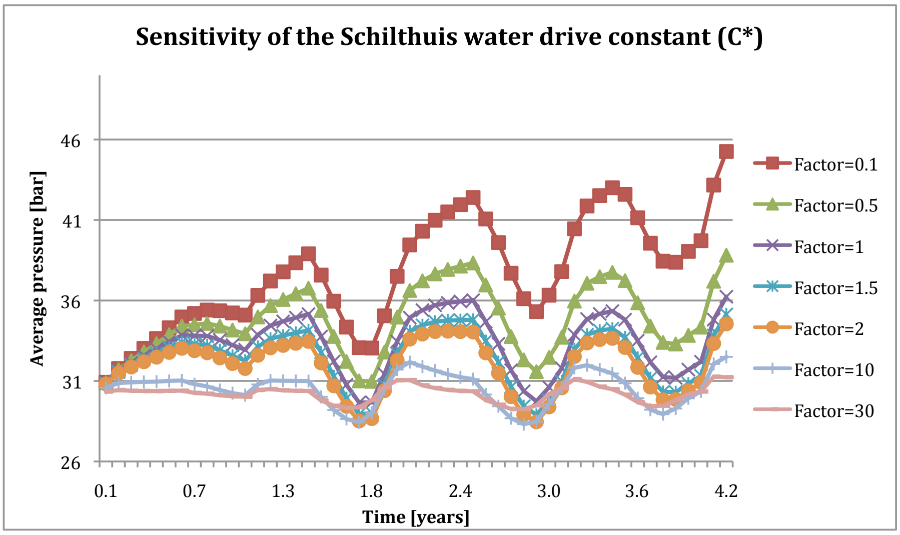

FIGURE 5.1: Sensitivity of the Schilthuis water drive constant with respect to different percentages of the original value of C^* from Reservoir A.

Production/Injection Rate:

In this implicit method, the time steps is originally divided into months where dt=0.084 years, which responds to a time step of one month. In this section, sensitivity of the time step has been done for time steps similar to half a month and two months, which respectively are equivalent to dt=0.042 years and dt=0.168 years.

Figure 5.2 shows a plot of two pressure functions with respect to time when the time step is similar to dt=0.16 and dt=0.08. Figure 5.3 shows a plot of two pressure functions with respect to time when the time step is similar to dt=0.04 and dt=0.08.

There is a variation in the pressure functions where the time step value is half of the original value. The smaller time step, dt=0.04, gave almost the same pressure trend as for the original time step, but the graph appears to be time-shifted.

A time step of two months give a less detailed average pressure function, while a time step for every half months gives a detailed result of the average pressure function. These parameters affect the average value of the pressure to a small extent, and are not an important parameter.

Gas Entrapment Factor (F_g):

The gas entrapment factor (F_g), is a measure of how much of the gas that will

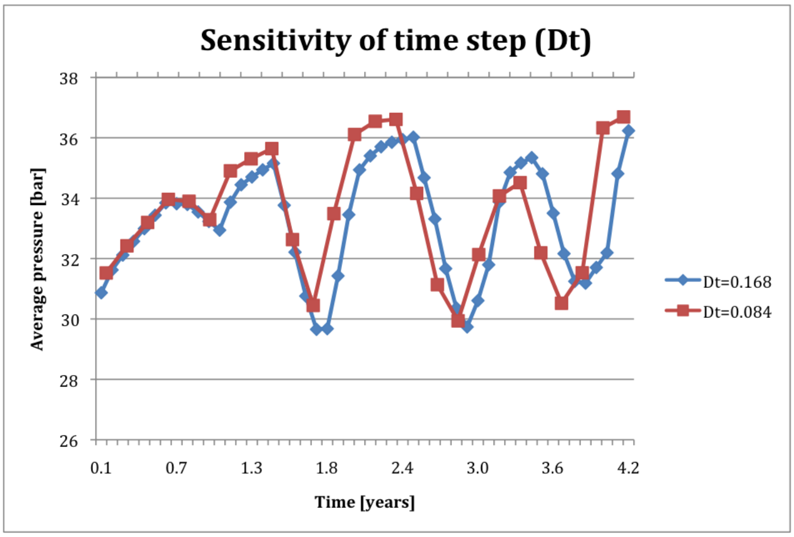

FIGURE 5.2: Sensitivity of time step (Dt). Average pressure versus time is shown for dt= 0.168 and dt=0.084.

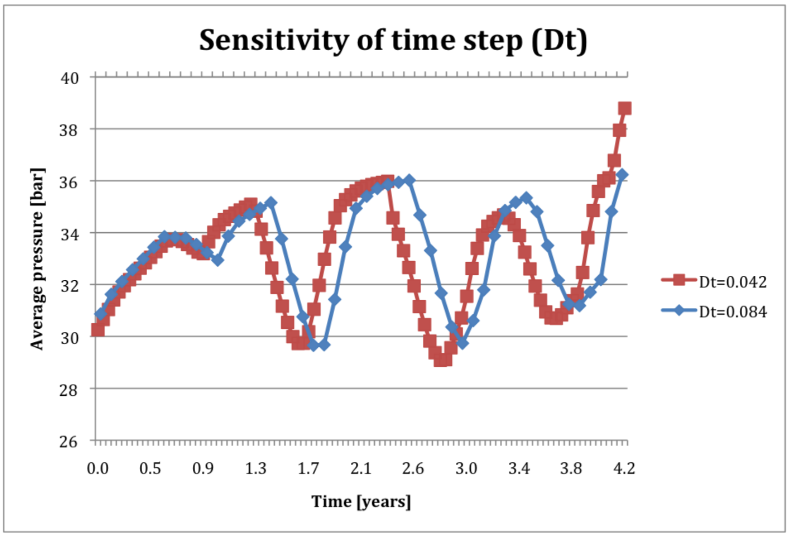

FIGURE 5.3: Sensitivity of time step (Dt). Average pressure versus time is shown for dt=0.042 and dt= 0.084.

be entrapped during injection and production. The original value of the gas entrapment factor is similar to F_g=0.003, but the parameter has also been tested for F_g=0 and F_g=1. Figure 5.4 shows a slightly more pronounced pressure function for low values of F_g.

The equation below shows that F_g exist for values between 0 and 1, and tell how large the volume rate of trapped gas will be due to how large the rate of water influx, $\dot{W}_e$ into the reservoir is.

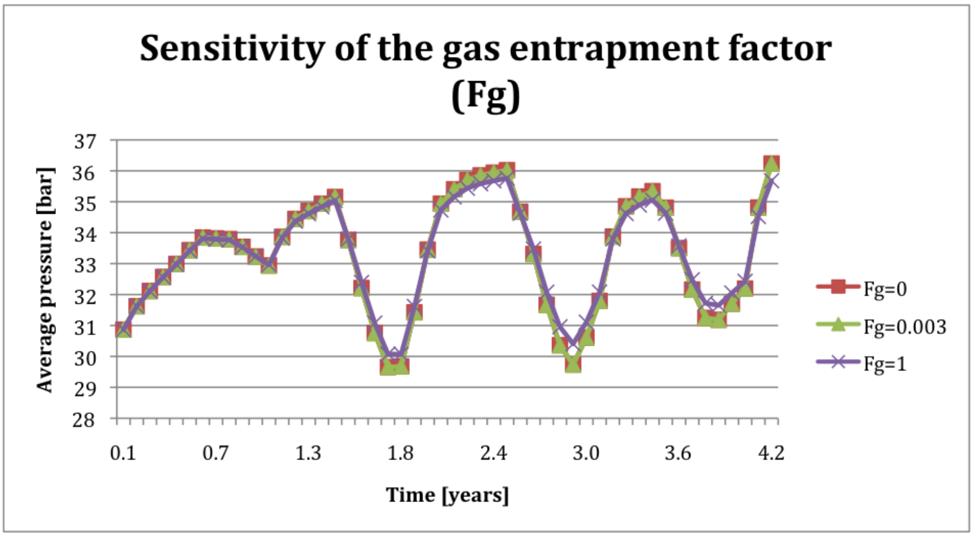

FIGURE 5.4: Sensitivity of the gas entrapment factor with respect to its pressure, tested in Reservoir A.

$$\dot{V}_T = F_g \dot{W}_e \tag{3.3}$$

Low values of F_g let almost no gas be trapped in the reservoir.

In order to get a better understanding of how different values of F_g affect the trapped volume of gas in the reservoir, $\dot{V}_T$ versus time has been calculated and plotted in figure 5.5.

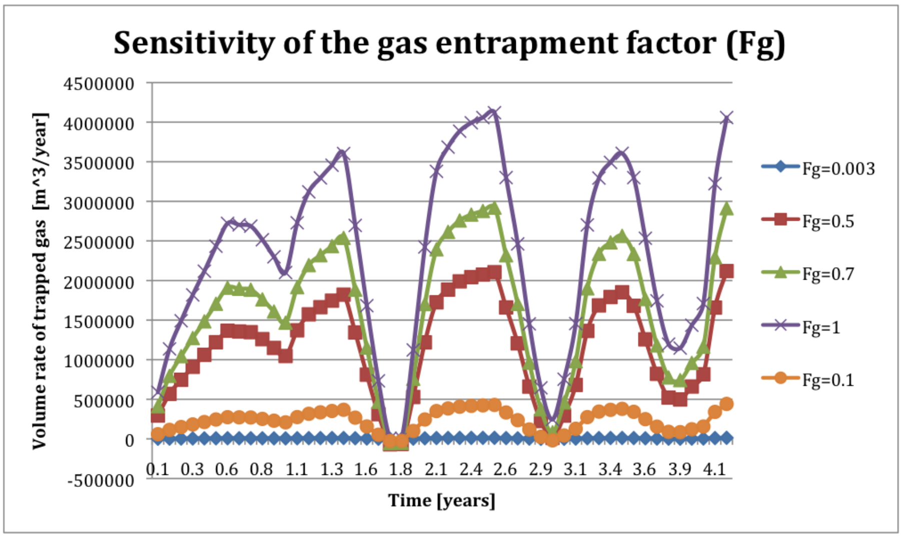

FIGURE 5.5: Sensitivity of how the volume rate of trapped gas, $\dot{V}_T$ respond to different values of the gas entrapment factor F_g.

From observations of how the volume rate of trapped gas, $\dot{V}_T$ depends on the gas entrapment factor, F_g, there is seen that F_g is an important factor. When F_g=0, the volume rate of water influx, $\dot{W}_e$ do not affect the amount of trapped gas. When F_g=1, $\dot{V}_T = \dot{W}_e$, which is unlikely. The volume rate of gas being residually stored is not as great as the volume rate of water influx flowing into the reservoir. The water influx into the reservoir may encroach just a portion of the gas at the contact zone. The general trend of figure 5.5 is that the curves change according to the cyclic injection and production rate q(t).

Initial Pressure (p_i)**:**

Sensitivity has been run on the initial pressure. Figure 5.6 shows how the pressure function varies with different values of the initial pressure. A low initial pressure in the reservoir, give lower pressure functions, which is less pronounced.

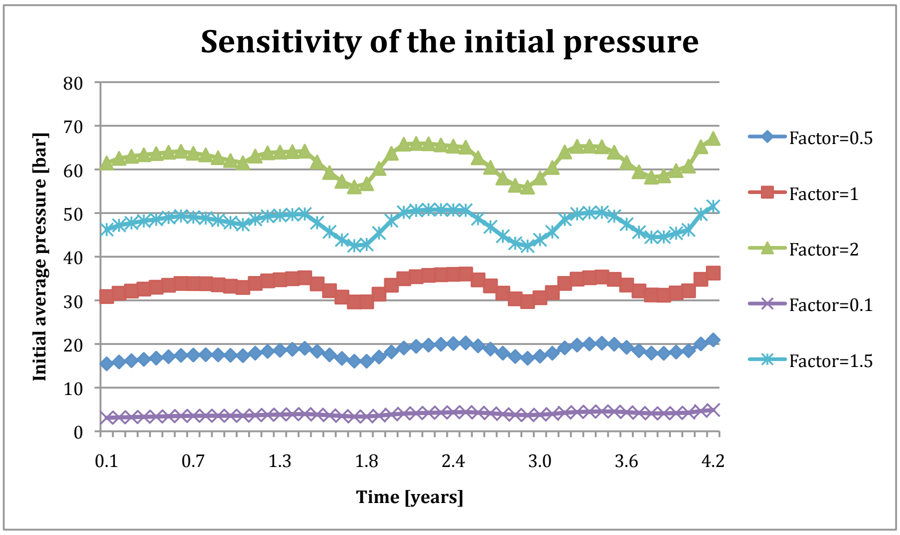

FIGURE 5.6: Sensitivity of the initial pressure with respect to different values tested in Reservoir A.

The ideal gas law, related to the density, shows how the density of the gas is related to the average pressure in the reservoir:

$$\rho = \frac{G}{V} = \frac{p}{RT}.$$

The gas compressibility, c_T is shown by:

$$\boxed{c_T = \frac{1}{p}} \tag{5.1}$$

where

$$c_T = \frac{\frac{d\rho}{dp}}{\rho}$$

If the initial pressure in a reservoir have increased, equation 5.1 shows that the compressibility decrease. Because the gas in the reservoir is less compressible, a larger pressure, more exact a larger $\triangle p$ $(p_{well} - p_{init})$ is needed in the reservoir in order to inject and produce the desired amount of gas.

Since all cases for the Collier model uses the Sm^3/day production/injection rate, cases with an increase in p_i will then inject less volume than for lower p_i.

Initial Amount of Gas in Place (G_i):
Sensitivity analysis of the initial amount of gas in place, G_i, has been done for a range of values from 10% of the original G_i, to twice as big as G_i. This analysis showed an increase of a more pronounced pressure graph when G_i was decreased, see figure 5.7. When G_i, was increased, a less pronounced pressure graph was shown.

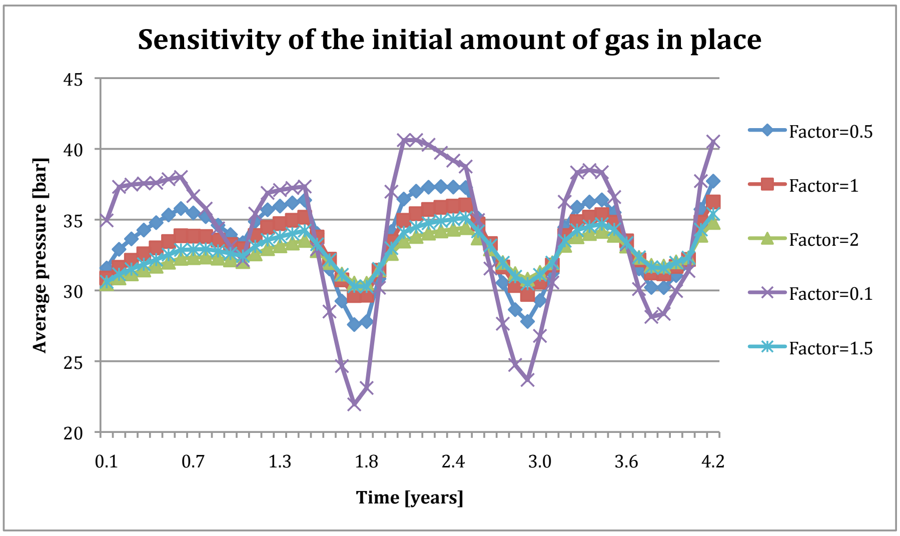

FIGURE 5.7: Sensitivity of the initial gas in place with respect to its pressure, tested in Reservoir A.

The value of the initial amount of gas in place, G_i have a large impact on the pressure injection/production graph. When the initial amount of gas in place is small, a large pressure difference between the bottom hole pressure and the initial pressure will occur during a cyclic period in order to inject and produce the gas. When the value of the initial gas in place is high, less pressure difference between the bottom hole pressure and the initial pressure is needed in order to inject and produce the desired amount of gas.

5.2 Observations from the Sensitivity Analysis

Necessary sensitivity analysis has been done on the implicit method. The most important observations are listed below.

Observations:

- After the sensitivity analysis of C^*, it is clear that C^* has a major role.
- The value of F_g range between 0 and 1, and tells how large the volume of trapped gas will be compared to how big the volume rate of water influx into the reservoir is. A value of F_g similar to 0.003 therefore appears to be an appropriate value where almost no gas is trapped.
- When it comes to the initial pressure, it is the pressure difference between the pressure in the well, p and p_i that is important. An increase in p_i lead to lower compressibility in the reservoir, and the pressure difference therefore need to increase in order to inject the desired amount of gas.
- The sensitivity analysis of the time step, dt showed that no significant improvement could be done by changing the dt.
- The value of the initial amount of gas in place, G_i have a large impact on the average pressure graph.
- The sensitivity analysis shows that the implicit method differ from the Collier model.

Tuning to Match Collier Data:
Because of the difference between the re-created implicit method and the Collier model, a factor x was multiplied to the model in order to see if that would reproduce a more similar graph. If for example the x-value corresponds to a change in the initial gas in place parameter of 1 percent of its original value, and

the Schilthuis water drive constant was changed to be 40 percent of its original value, the new average pressure graph would be almost similar to the one from the Collier′s paper. This is seen in figure 5.8.

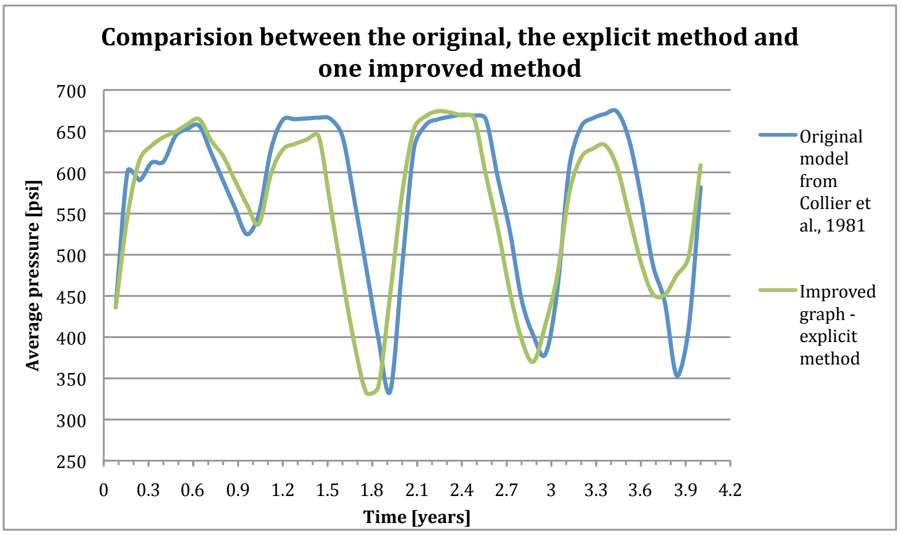

FIGURE 5.8: Comparision between the improved graph based on the implicit method and the graph from Collier's paper after changing the value of G_i and C^*.

6. Eclipse Simulations

6.1 The Eclipse Simulator

The reservoir simulation software Schlumberger Eclipse 100 has been applied in this section to simulate for reservoir behaviour. FloViz is used to get a visual picture of the geology, and to display saturation distributions.

6.2 Description of the Comparison between Collier and Eclipse

In order to test sensitivity of different parameters to the difference of cyclic storage between methane and CO_2, a base case homogenous model was made, see figure 6.1. Similar for all the models are the porosity, grid block dimensions, placement of perforations in the well, well placement, and saturation functions.

The number of active grid blocks were 56250 cells, were each grid block has the size of 20.84m in the horizontal direction, and 10m in the vertical direction. The model is formed like an anticline with the top at 415m depths. In the Collier model, the depth of the anticline was at 415m. Since the model in eclipse later should work for storage of CO_2, which work best for depth lower than 800m, a new depth of the anticline was later moved to 1000m. The anticline bends 100m down to the sides. Production and injection well were placed in the middle of the model with perforations in the top layer. The oil in the model was given water properties, while the gas was given methane or CO_2 properties. The reason for letting water alias for oil is that it facilitates the properties of dissolution of gas in the liquid fluid. This effect of residual stored gas is shown in figure 6.2.

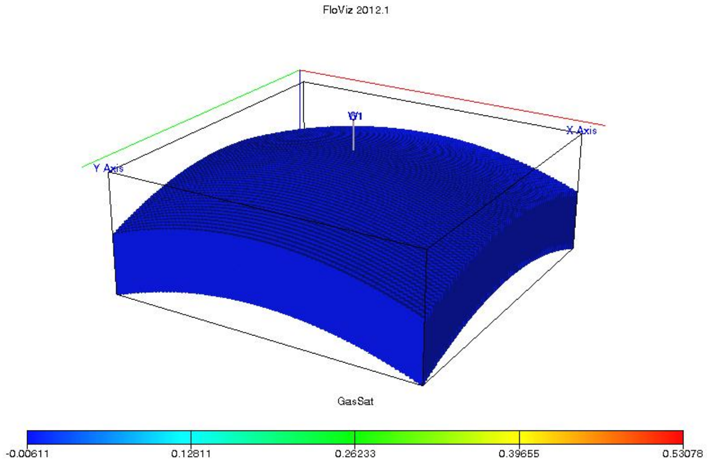

Figure 6.1: Base case geometric model from FloViz.

From figure 6.2, relative permeability curves are shown for both water and gas during the first cycle. The gas is either methane or CO_2. At the beginning, there is 100% water in the reservoir. Then, gas is injected into the reservoir, and one gets drainage of water. After 6 month when injection is over, 25% water is stored residually in the reservoir. Then, production of gas starts. It is important to note that water may also be produced. During production of gas, some of the gas is trapped, and at the end of production, only 40% of the gas is produced.

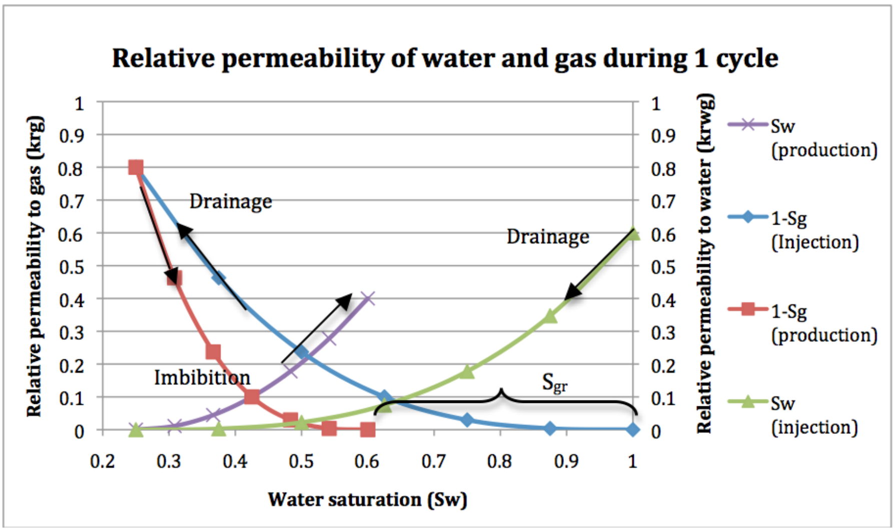

Figure 6.2: Relative permeability of gas and water versus water saturation during 1 cycle.

6.2.1 Simulation Result of Modelling Natural Gas Reservoir Based on Collier et al., 1981.

A model for modelling natural gas reservoirs was made in chapter 3. This chapter shows the simulated result of the model based on Collier et al., 1981. Figure 6.3 shows the results after simulations compared to the one in Colliers paper. The model is concluded to be a good enough match, even when the first spike around t= 1 year, did not appear clearly at the simulations.

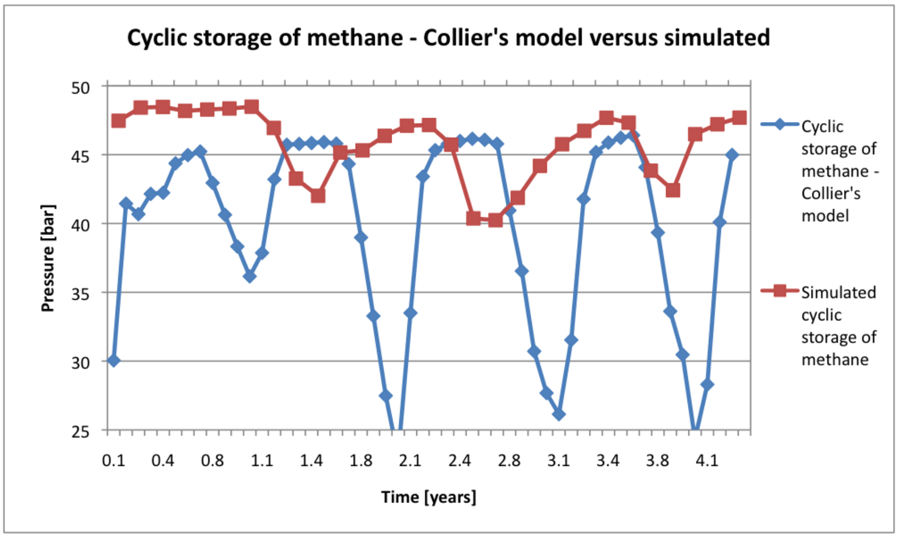

FIGURE 6.3: Cyclic storage of Methane from Collier et al., 1981. compared to the simulated model. Average pressure is shown during each cycle. Note that the first clearly spike appears after two years for the simulated model; the pressure response after one cycle is not represented.

As discussed, the model in Collier's paper is a 0-dimensional simplified formulation. Eclipse simulation based on this model depends on several factors which not the 0-dimensional model does. The Eclipse model is a 3-dimentional homogenous model, and opposed to a 0-dimensional model, one needs to define transport properties such as absolute porosity and relative permeability for the reservoir model.

6.2.2 Rate R(t)

The modelling and simulations have been based on the example case in Collier et al., 1981, in the previous sections. When it came to do simulations in order to compare methane cyclic storage with CO_2 cyclic storage, a more generalized simulation model was needed. It was necessary with a new rate function.

Equation 6.1 shows the generalized rate function used in the base case for storage of methane and CO_2. c is a constant similar to $5.17x10^6$ m^3/day^2.

$$R(t) = c \cdot \sin\left(2\pi \frac{t}{T}\right) \tag{6.1}$$

where T is the period similar to 1 year.

It will be easier to compare different gases when each cycle has the same injection and production rates.

6.2.3 Cyclic Storage of CO_2

A base case for cyclic storage of CO_2 was made, and the rate function R(t) was used. Figure 6.4 shows the base case of cyclic storage of CO_2 during 4.2 years.

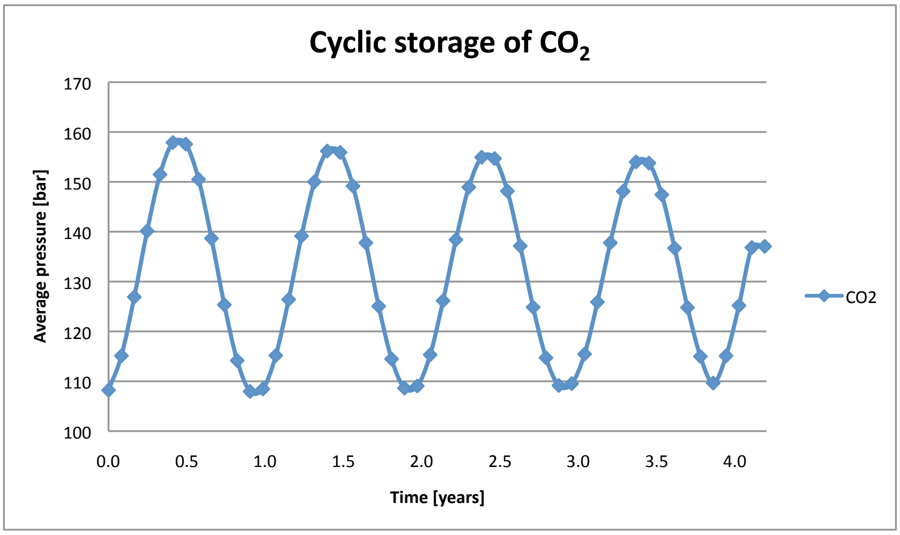

FIGURE 6.4: Field reservoir pressure versus time for the base case cyclic storage of CO_2.

CO_2 has a strongly varying density as a function of pressure. Approximately critical depth for storage of CO_2 is at 800m. Below this depth, CO_2 will be stored as a supercritical fluid where it is much denser than above the critical depth. The depth used for the CO_2 model was therefore set to be at 1000m.

6.2.4 Deeper Storage of Methane

Want to simulate methane storage at 1000m depth, which will be more comparable to storage of CO_2 at the same depth. Figure 6.5 shows the base case cyclic storage graphs that will be the starting point for further simulations. The difference in pressure reflects that methane and CO_2 are two gases with different properties. Figure 6.6 compare the reservoir volume of gas in place of methane and CO_2. During each cycle, the volume gas of CO_2 was lower than for methane. After three years, the volume increased to be the same as for methane.

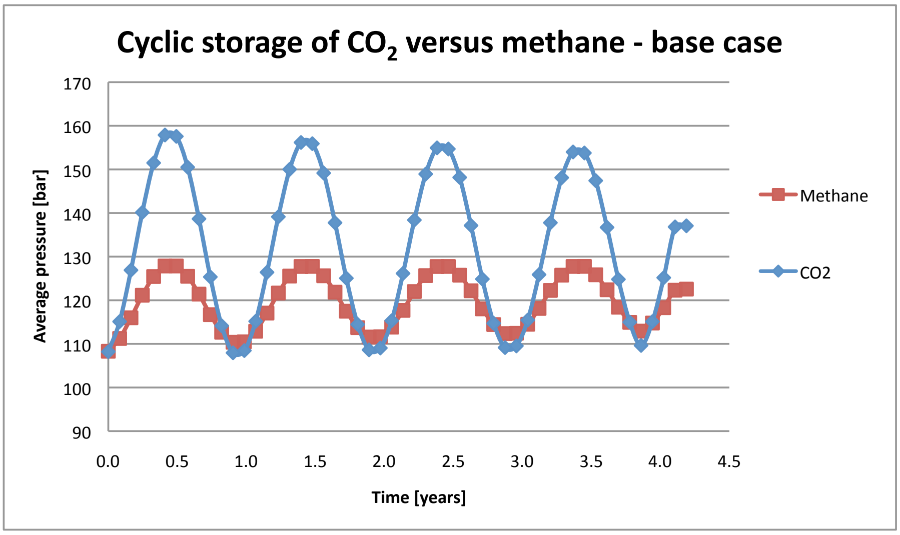

FIGURE 6.5: The base case cyclic storage graphs of methane versus CO_2. Methane and CO_2 shows different pressure curves, even when the geology for cyclic storage was the same.

When CO_2 versus methane is injected, methane is injected with lower pressures, while CO_2 need higher pressures. The fact that methane is in a gas state, while CO_2 is in a liquid state plays a role. The total compressibility for methane is higher than for CO_2. This is seen in figure 6.7 . To illustrate this effect, equation 6.2 shows how the reservoir volume is related to the compressibility of the gas:

$$Q = c_T \triangle \overline{p} V_{por} \tag{6.2}$$

In the equation, Q is the reservoir volume injected or produced, c_T is the total compressibility , $\overline{p}$ is the average pressure in the reservoir and V_{por} is the pore volume.

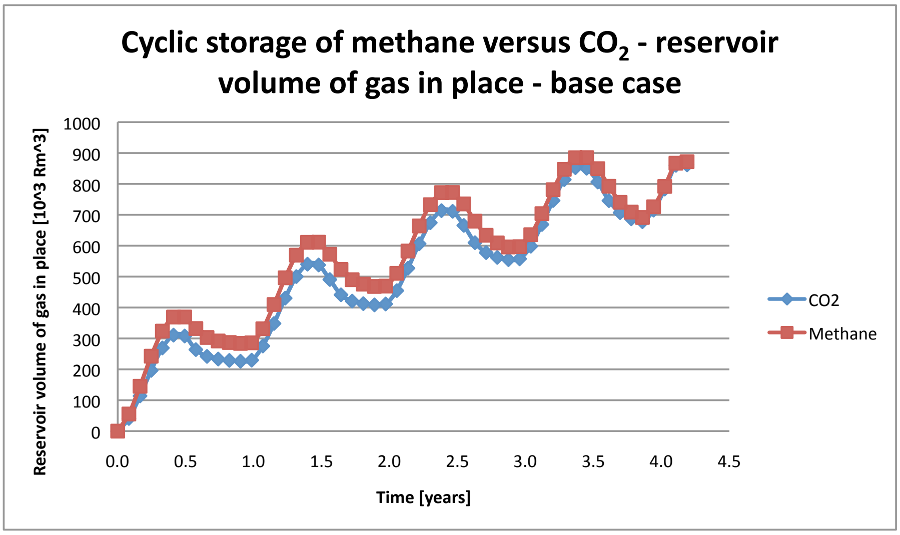

FIGURE 6.6: The base case cyclic storage graphs of methane and CO_2 when it comes to different amounts of gas in place in the reservoir versus time.

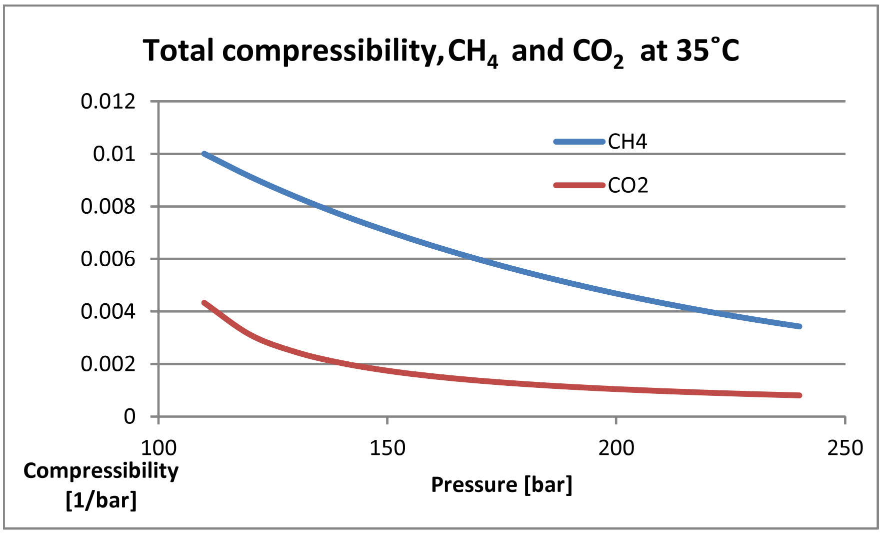

FIGURE 6.7: Total compressibility of methane and CO_2 at 35°C.

Note the general trend where the volume of gas in place for both methane and CO_2 in 6.6 increases with time. While looking at the graph, no noticeable signs differ methane and CO_2 from each other. As mentioned above, the average pressure response from each of the gases in figure 6.5, were different. In the data file for simulation, injection and production were controlled by reservoir volume rate. The initial pressure was set to be 100 bars. Figure 6.8 shows the base case of the bottom hole pressure responses during injection and production during each cycle with time.

When looking at figure 6.8, the blue points are showing the injection pressure during the first 6 months before production takes over for the next 6 months,

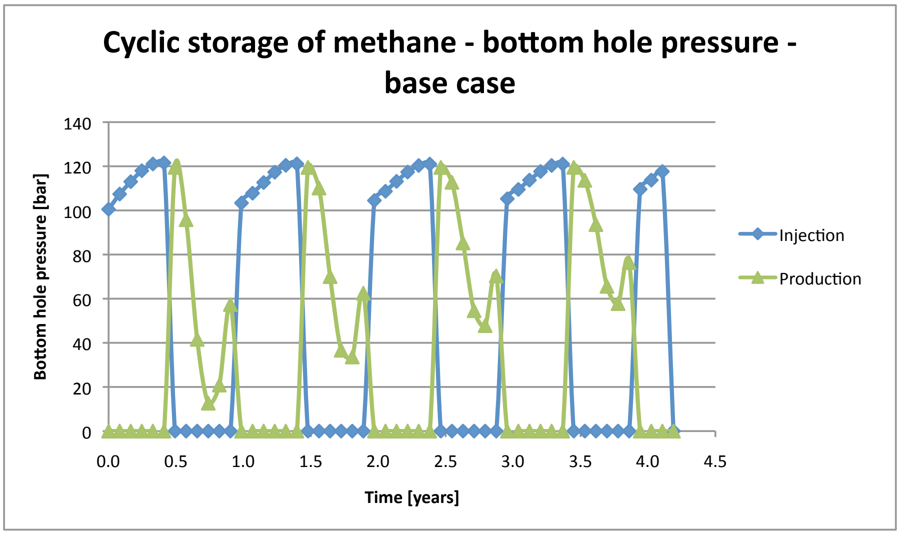

FIGURE 6.8: Cyclic storage of methane showing the bottom hole pressures for injection and production with time.

and so on. Note the initial pressure at 100 bars, and those pressure points lower than this value results in production. The maximum pressure during injection reached about 120 bars, and repeated itself for every cycle. The lowest production pressure for each cycle varied, were it was lowest after the first cycle, and gradually increased upward with time. The viscosity of methane and CO_2 is significant. An example of the different viscosities at 100 bars are:

- = Viscosity methane: 0.0219 mPa s
- = Viscosity CO_2: 0.063 mPa s
- = Viscosity water: 0.758 mPa s

The viscosity of methane and CO_2 increase with increasing pressure, while the water viscosity hardly change. The observation is that methane and CO_2 have lower viscosity than water, and during each cycle, it gets more and more gas into the reservoir. As a result of more gas, the total water + gas movement in the reservoir gets less viscous, and it ”flows easier”. Less production pressure is therefore needed in order to inject the desired amount of gas after each cycle.

The base case of the bottom hole pressure responses during injection and production for CO_2 had almost the same trend as for methane. See figure 6.9. The pressure during injection of methane reached almost 160 bars during each cycle, while the minimum production pressure needed in order to produce CO_2 decreased to about 10 bars. During each cycle, the minimum production pressure increased for each cycle, but not as fast as for methane. The effect of differences in viscosity and compressibility is seen here. Because CO_2 have higher viscosity than methane, higher production pressures is needed.

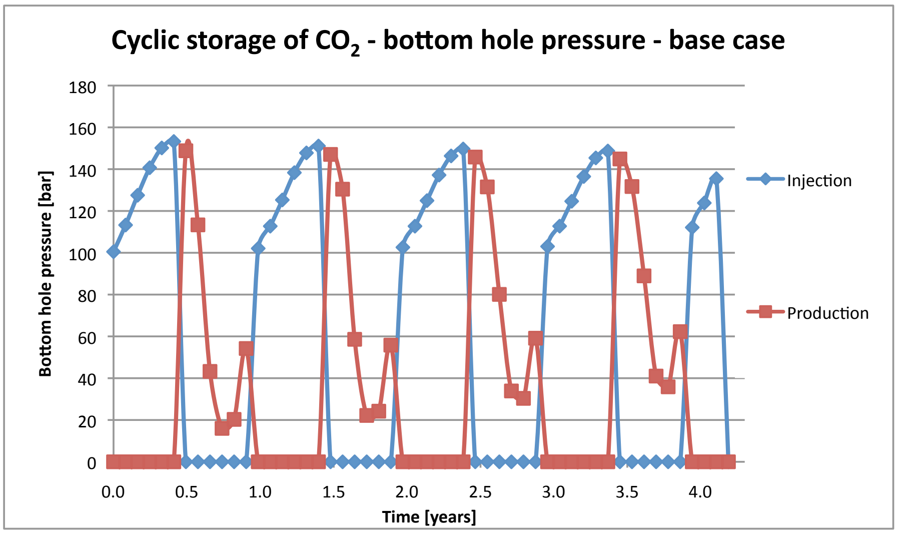

FIGURE 6.9: Cyclic storage of CO_2 showing the bottom hole pressures for injection and production with time.

6.3 Sensitivity of methane storage versus CO_2 storage

In this section, sensitivity of methane storage versus CO_2 storage is done. Table 6.1 shows the different simulation cases. All the cases have been simulated with the same injection and production rates.

6.3.1 Residual Trapping

A definition of hysteresis is: what happens next also depends on history and not only the current state the reservoir is in. Figure 6.2 shows the general plot of relative permeability of water and gas during one cycle with hysteresis. The effect without hysteresis is shown in figure 6.10.

In the case with hysteresis, there is seen in figure 6.2 that one gets a value of the residual saturation of gas, S_{gr}, while in the case without hysteresis, the value of S_{gr}

Table 6.1: The different simulation cases

Simulation Cases	
Sensitivity of parameters	**The different cases**
Permeability:	1) Permeability = 500mD (base case)
	2) Permeability = 50mD
Aquifer pressure support:	1) Permeability of the reservoir
	and the aquifer = 500mD (base case)
	2) Permeability of the reservoir = 500mD,
	permeability of the aquifer = 5mD
Geometry:	1) Hight of the anticline structure = 100m
	2) Hight of the anticline structure = 50m
Dissolution:	1) Dissolved gas at 1000m
	2) Without dissolved gas at 1000m
Residual trapping:	1) With hysteresis
	2) Without hysteresis

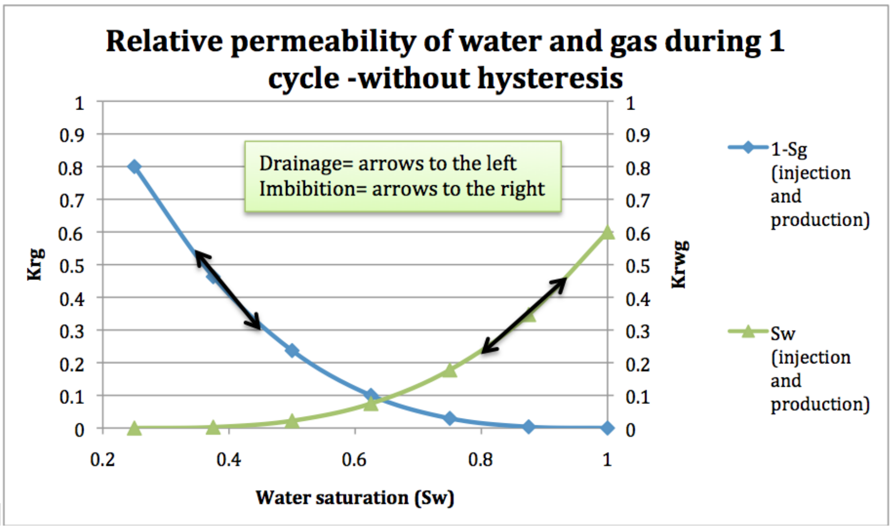

Figure 6.10: The general relative permebility of water and gas during 1 cycle without hysteresis.

is not taken into account. In the case without hysteresis, the drainage curves are similar to the imbibitions curves, just that they work in the opposite directions.

To illustrate the effect of residual saturation during cyclic storage of methane and CO_2, the use of hysteresis versus without were used. One case was simulated for methane with and without hysteresis. Figure 6.11 shows the pressure graphs, which is almost identical. The only difference is that the pressure curve for methane with hysteresis does not decline as much as for the pressure curve without hysteresis. Compared to CO_2, it is not any noticeable difference other than that CO_2 is slightly more similar to the base case than methane due to the difference in compressibility.

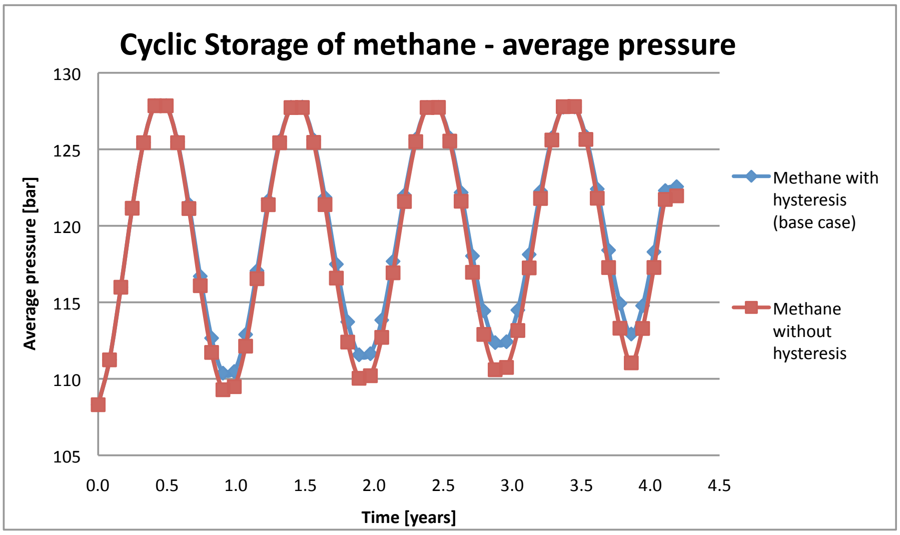

FIGURE 6.11: Cyclic storage of methane with and without hysteresis. The average pressure with time is shown.

Figure 6.12 shows the reservoir volume of gas in place for methane with and without hysteresis. This graph clearly shows the impact the hysteresis has on residual trapping. After every cycle of storage, more methane is trapped for both the cases, but to a greater extent for methane with hysteresis.

Figure 6.13 shows the reservoir volume of CO_2 in place. The effect of hysteresis on volume of gas in place is identical while comparing 6.12 and 6.13. Another important observation is the produced water. At the first cycle, before injection of gas, it was only water in the reservoir. After 6 month of injection of gas, both water and gas started to be produced, even when the goal was to just re-produce the gas. During the next cycle, more gas was injected, and during the production, less water was now produced due to higher volume of gas in the reservoir. Figure 6.14

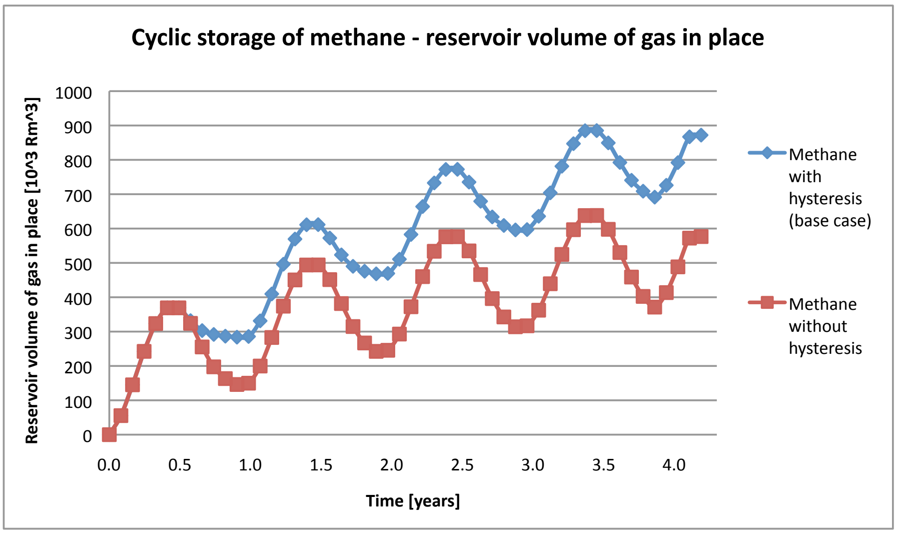

FIGURE 6.12: Cyclic storage of methane with and without hysteresis. Showing the differences in reservoir volume of gas in place with time.

shows the water production rate curve for cyclic storage of CO_2, which illustrate that less and less water is produced with time. Figure 6.14 shows that water is being produced both for the case with hysteresis, and without. With hysteresis, more water is being produced, and this trend is supported by the trend in the reservoir volume figures of both CO_2 and methane where the base case for stored gas was higher.

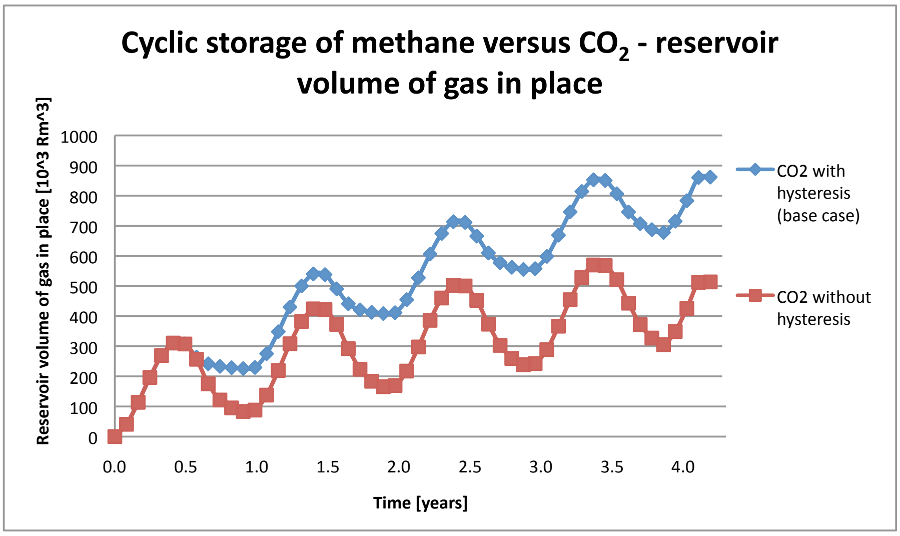

FIGURE 6.13: Cyclic storage of CO_2 with and without the effect of hysteresis. The difference in reservoir volume of gas in place in shown with time for the two cases.

Back to the observations of figure 6.13 and figure 6.12. The general trend shows that the reservoir volume of gas in place increases gradually after each cycle. The

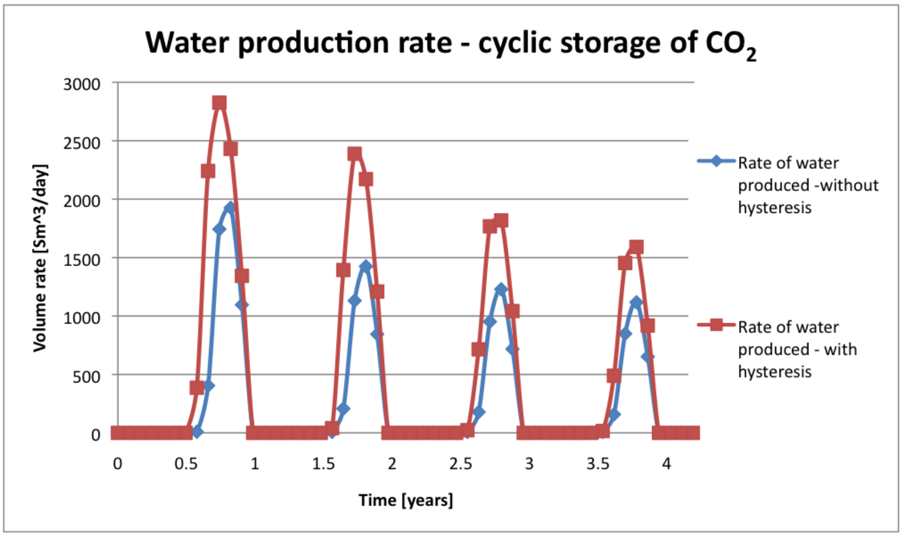

FIGURE 6.14: Volume rate of produed water with time.

ideal case would be that the same amount of gas was injected and produced. The case is that the hysteresis effect does that some of the gas is residually trapped. The other case is that the production volume rate is similar during each cycle, and since water is being part of the production, less gas is produced.

6.3.2 Degree of Pressure Support

The water in the aquifer will have a force upward on the reservoir where gas is stored temporarily, especially during production of gas. If the permeability of the aquifer changes, it may affect the storage capacity, and the injection and production pressure may change. Case 1 is the base case where both the reservoir with gas and the aquifer has the same permeability of 500mD. In case 2, the aquifer has a lower permeability of 5mD. The gas-water contact may vary, but in this case, the top of this aquifer is set to a depth of 1020m for simplicity.

When the permeability of the aquifer is decreased, the pressure in the reservoir also decreased and less methane and CO_2 was stored. Figure 6.15 and 6.16 shows the reservoir pressure during 4.2 years of cycling storage. By comparing how the pressure functions decreased, differences between the gases are seen. When the permeability decreased to 5mD in the aquifer for storage of methane, the pressure function dropped with an average of 4 bars. Less methane was stored.

For CO_2, the pressure function reached higher pressures than for methane. If the base case is compared to case 2, where the permeability is lower in the aquifer,

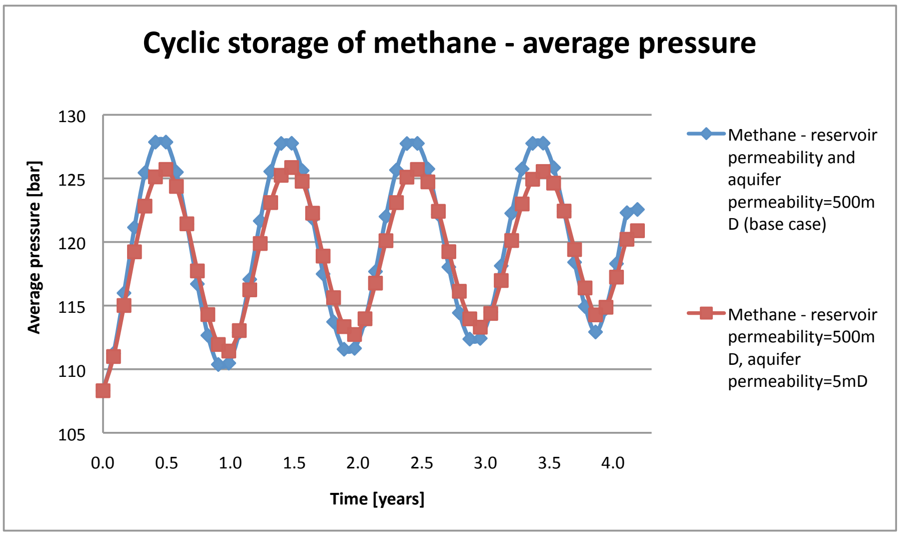

FIGURE 6.15: Reservoir pressure versus time for cyclic storage of methane when the aquifer pressure support was taken into account.

some differences are seen. The top pressures were the same, while the bottom pressures deviated slightly. The base case pressure decreased with about 2 bars at the end of each cycle compared to the second case.

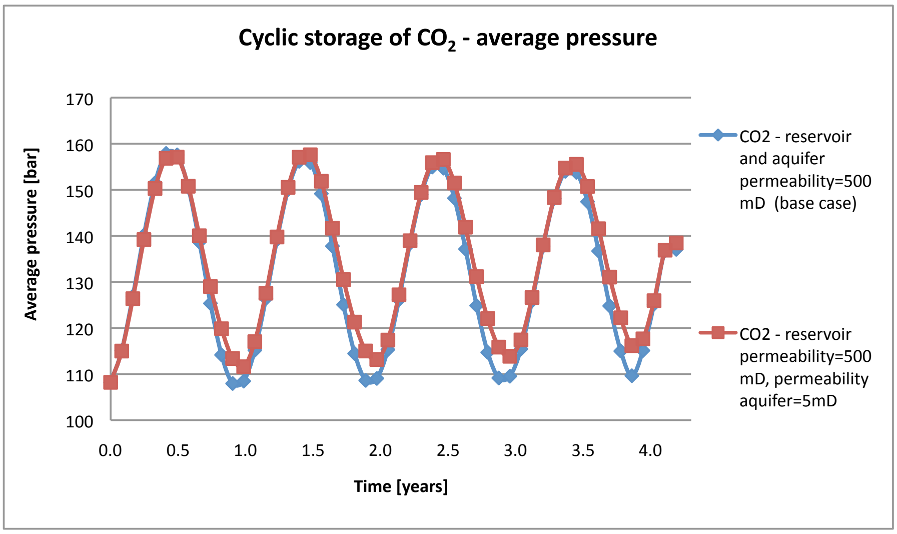

FIGURE 6.16: Reservoir pressure versus time for cyclic storage of CO_2 when the aquifer pressure support was taken into account.

Figure 6.17 and 6.18 shows how the reservoir volume of gas in place for both methane and CO_2 vary with time. For methane, the base case where the aquifer had high permeability resulted in general increasing reservoir volume of methane with time.

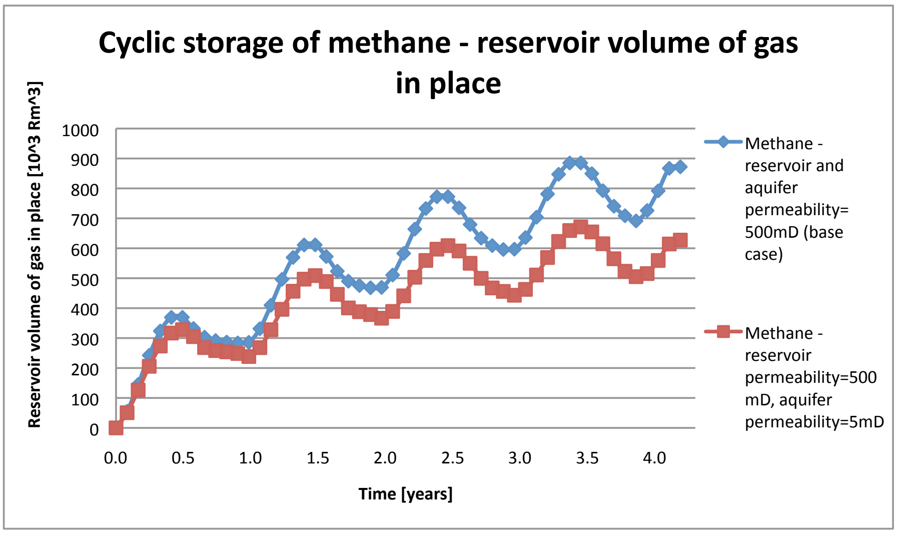

Figure 6.17: Volume of gas in place versus time for cyclic storage of methane based on aquifer pressure support.

For CO_2, the base case did not differ too much from the second case. Out from the two figures, the base case is almost the same, while the reservoir volume of methane deviated most from base case. More CO_2 than methan was stored.

At this depth, CO_2 is a supercritical gas; given liquid properties. Diffusion of CO_2 is higher than for methane, and it may result in more stored CO_2 at lower permeability because methane do not diffuse into low permeability layers as easy as CO_2.

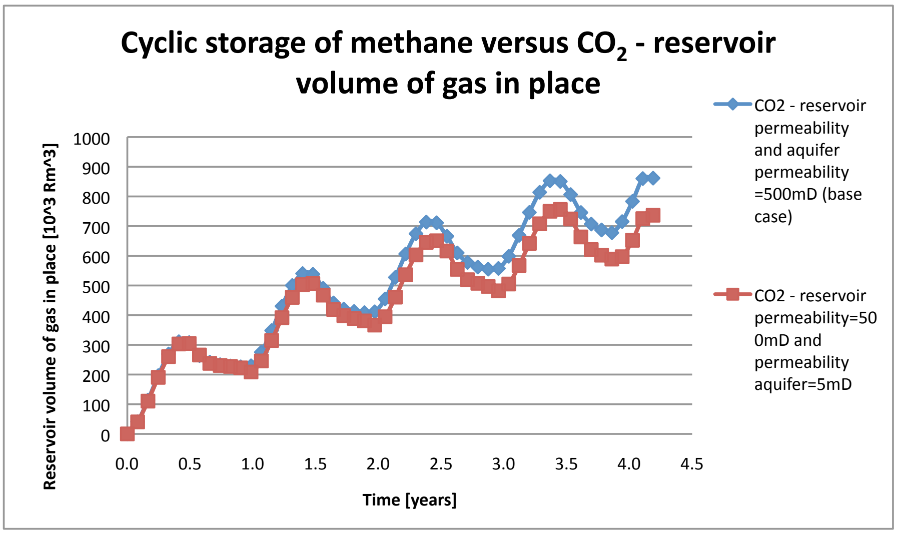

Figure 6.18: Volume of gas in place versus time for cyclic storage of CO_2 based on aquifer pressure support.

Like described in figure 6.2, the effect of hysteresis in the reservoir is present. When the permeability is high in the aquifer, $\dot{W}_e$ flow more easily into the reservoir, and results in a larger gas-water contact area, which results in a larger value of trapped volume of gas. This was shown earlier in chapter 5 for sensitivity of the gas entrapment factor F_g, supported by 3.3. When the permeability in the aquifer is low, the gas gets less space to develop on, and the smaller gas-water contact results in less accumulation of gas.

The conclusion from this section is that methane is affected by a decrease in the aquifer pressure support, while CO_2 is slightly affected.

6.3.3 Geometry

A sealing cap rock is necessary for storage of gas. When the base case was an anticline structure cap rock of 100m from the top of the anticline and down to the end of the flank, a change in depth of the anticline to 50m slightly affected the cyclic storage of gas. Figure 6.19 shows the base cases of average pressure for methane and CO_2. Figure 6.20 shows how the base case changed after the geometry change of the anticline structure. Compared to the base case, no noticeable change were seen expect of a slightly decrease in total pressure of about 2 bars for both CO_2 and methane.

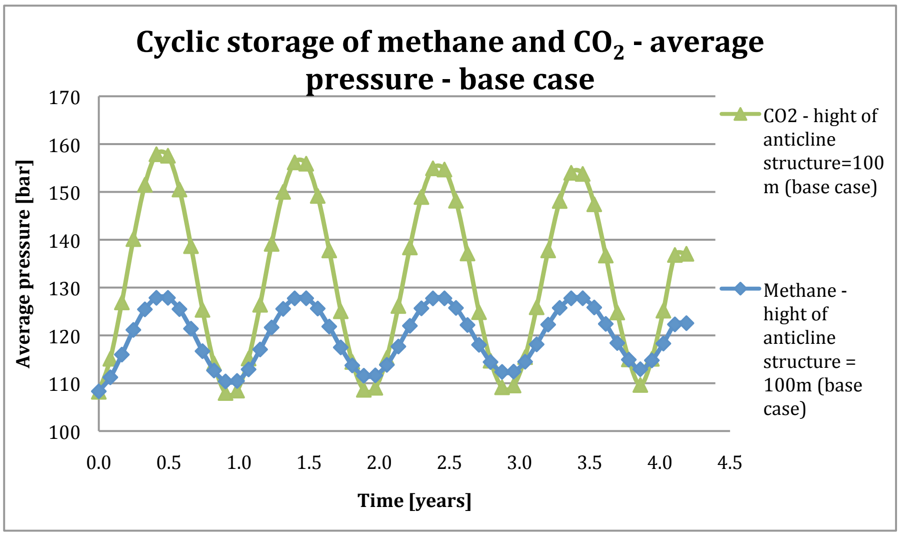

FIGURE 6.19: Average reservoir pressure versus time for cyclic storage of both CO_2 and methane.

For methane, this change in geometry resulted in a slightly increase in the volume of gas in place. This is seen in figure 6.21 where the volume of gas in place increased slightly faster for the anticline of 50m. The volume of gas in place for CO_2 did not change.

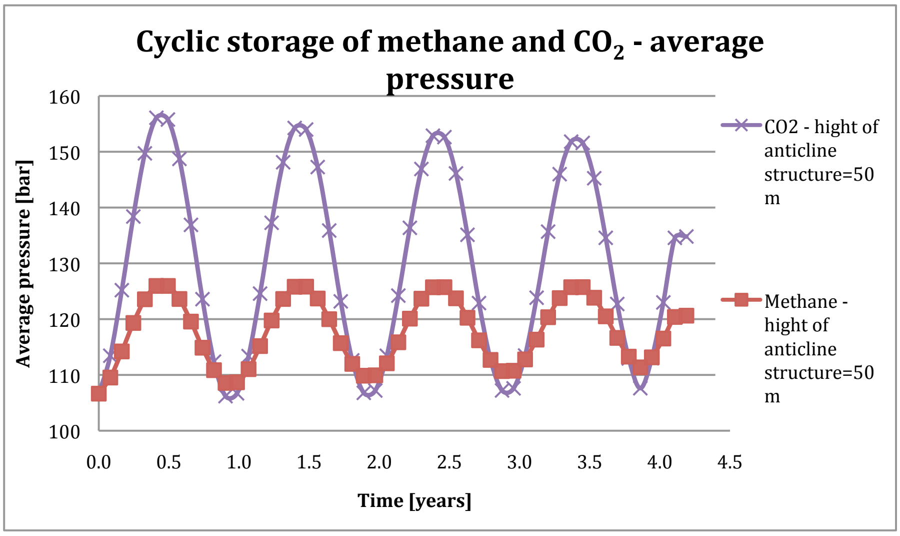

FIGURE 6.20: Reservoir pressure versus time for cyclic storage of both CO_2 and methane.

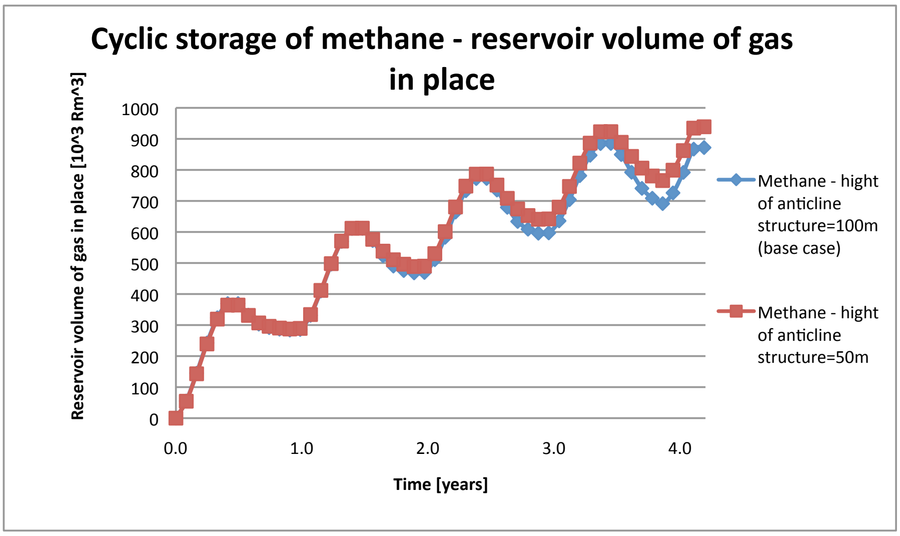

FIGURE 6.21: Reservoir volume of gas in place versus time during cyclic storage of methane. Two cases with different geometries are represented; an anticline geometry with depth of 100m (base case) and one of 50m.

The result of a change in the geometry did not affect CO_2, but it slightly affected methane. Overall, the trend of change for methane and CO_2 is similar, and the gases are in this case comparable.

6.3.4 Permeability

When the permeability decrease, the availability for the gases to enter pore spaces, decrease. More pressure is then needed in order to let the gas migrate through smaller pore throats. When the permeability decreases from 500mD to 50mD, the average pressure increases for both methane and CO_2 for each cycle. Figure 6.22 and 6.23 shows the pressure increase compared to its base case, both for methane and CO_2.

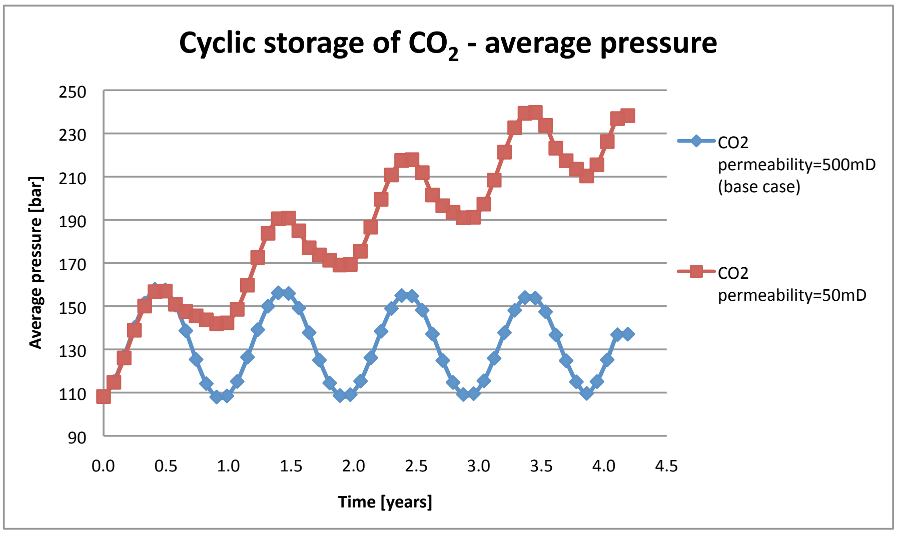

FIGURE 6.22: Reservoir pressure versus time for cyclic storage of CO_2.

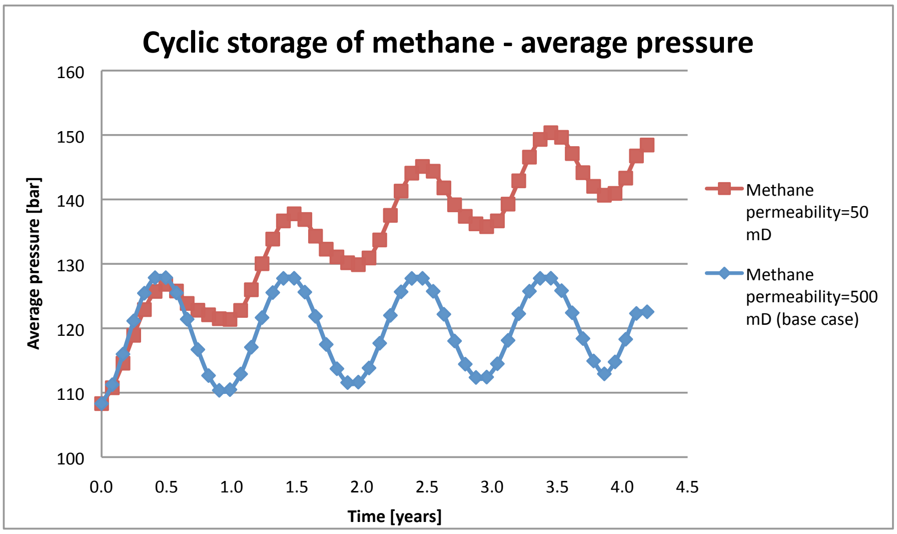

FIGURE 6.23: Reservoir pressure versus time for cyclic storage of methane.

The reservoir volume of gas in place for both methane and CO_2 did not change much after this drop in permeability. This is shown in figure 6.24 and 6.25. Note that the volume of CO_2 began to differ from the base case during cycle four, while methane was not.

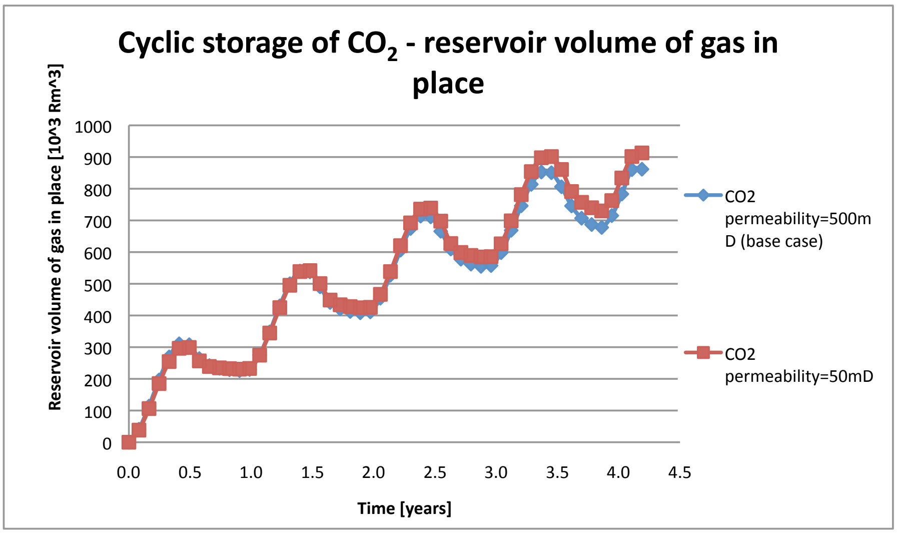

FIGURE 6.24: Volume of gas in place versus time for cyclic storage of CO_2.

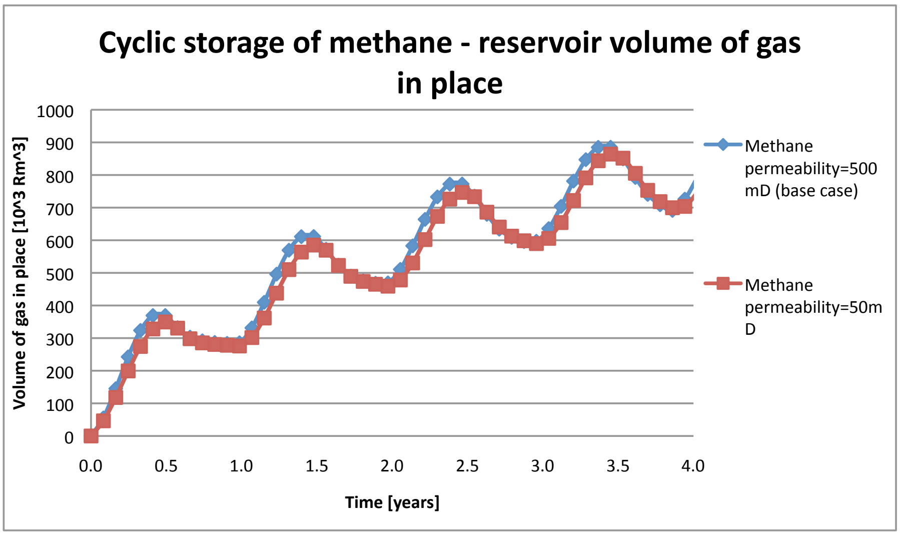

FIGURE 6.25: Volume of gas in place versus time for cyclic storage of methane.

The reasons for why the average pressure changed, but not the volume of gas in place, is because of the high target bottom hole pressure. For methane, the bottom hole pressure neither reaches the limited pressure for injection or production. Because of the lower permeability, these pressures get closer to the limits, and the average pressure in the reservoir increase.

The case for CO_2 was different. From the base case, CO_2 needed higher average pressures in order to inject and produce the desirable amount of gas due to the differences in compressibility of the two gasses. Figure 6.26 shows how the bottom hole pressure increases for each cycle of CO_2 to be injected. At the two last cycles, the pressure reaches the upper pressure limit of 300bars. This explains why figure

6.24 start to change the amount of CO_2 at the end.

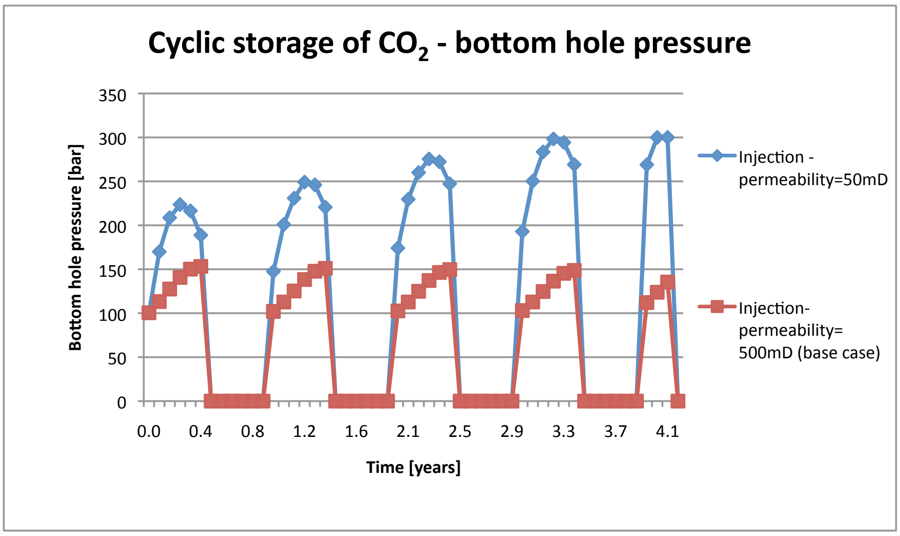

Figure 6.26: Cyclic storage of CO_2. Bottom hole pressure graphs for injection of the two cases.

Figure 6.27 shows how the bottom hole production for CO_2 behave compared to the base case. To produce the desirable amount of CO_2, the pressure drops fast down to the minimal bottom hole pressure limit of 1 bar.

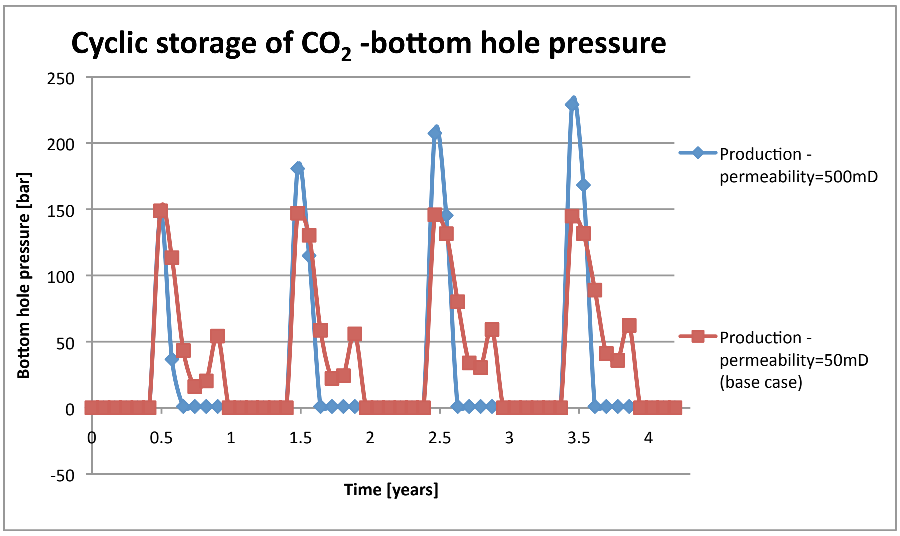

Figure 6.27: Cyclic storage of CO_2 showing the bottom hole pressures for production of the two cases.

The major observation from the sensitivity of permeability is that the permeability value in the reservoir is an essential flow parameter. CO_2 needs higher pressures in contrast to methane, in order to inject and produce the same desired amount. This is the case from simulation when the target pressures in the data file are set to be controlled by the bottom hole pressures, and not by the top hole pressures.

The weight of the CO_2 column in the well is higher than for methane, and results in pressures that needs to be taken into account during planning of a real cyclic storage project.

6.3.5 Dissolution

Dissolution of gas in water may cause "losses" of the gas during cyclic storage. Figure 6.28 shows the cases for cyclic storage of dissolved CO_2, and without dissolved CO_2. The time step used for the cases has been extended to show the increased effect of dissolution of CO_2 with time. The injection rates are similar each year, and the total pressure each year is also the same. From the figure, the temporarily stored CO_2, without taking account to any dissolved CO_2, shows a higher level of stored CO_2 in place. The other graph take into account an amount dissolved CO_2 in water which may be seen as loss of CO_2 during re-production. With time, the two graphs gets out of phase compared to each other, and the reason why is unclear.

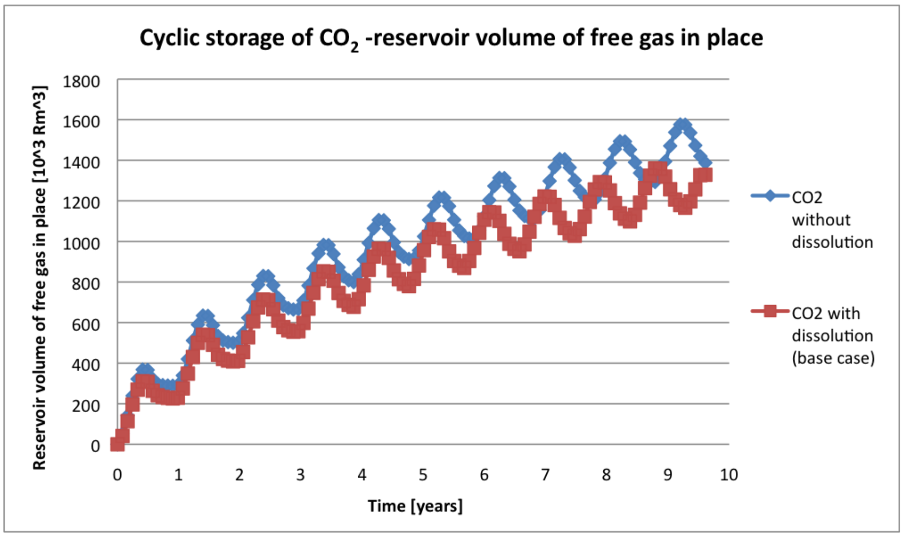

FIGURE 6.28: Volume of free gas in place versus time for cyclic storage of CO_2 with and without dissolution effects.

With time, more CO_2 will be dissolved in water. After the last cycles, the value of residual saturated gas has increased due to farther migration of CO_2 from the injection well during each cycle. Note that with time, both the graphs increase the volume of gas in place for each cycle. Compared to methane, CO_2 is usually stored as a supercritical fluid, where the gas is compressed significantly. Normally, the degree of dissolution decreases with temperature for gasses, except for CO_2.

It is assumed based on this theory that methane will not dissolve significantly enough in water, especially compared to CO_2. When methane dissolves in water, the water density will decrease. It is then not possible to take into account the gravitational disqualifications that works for CO_2.

From figure 2.1 in the review section, the injected gas is assumed to spread out to have a horizontal gas-water contact. The results from the simulations shown in FloViz shows a more dynamical shape of the injected CO_2. Figure 6.29 and 6.30 shows the residual saturated CO_2 that is trapped after one cycle, and after 10 cycles.

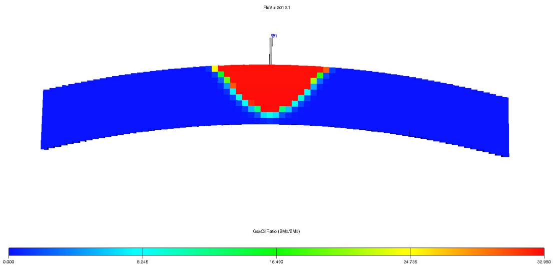

FIGURE 6.29: Residual saturation of CO_2 after one cycle of injection and production.

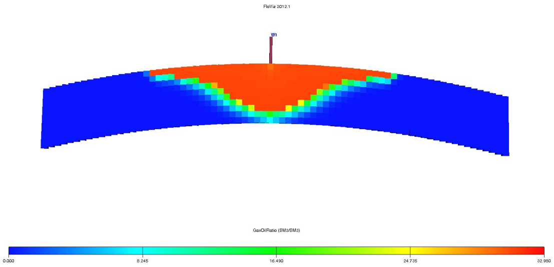

FIGURE 6.30: Residual saturation of CO_2 after 9 cycles of injection and production.

After one cycle, the injected CO_2 have been spread radially out from the injection point out in the aquifer, where the perforations both from injection and production was placed in the top layer. With time, when several cycles have been injected, the shape of how CO_2 is formed in the aquifer has changed. In earlier sections, the effects of water support from the aquifer have been analysed. If the pressure support from the aquifer was less, less CO_2 was stored. The pressure support was dependent of the permeability of the layer, and therefore, the permeability of the layers below the injection- and production point is important. The effect of the geometry described in the section above for CO_2 concluded that the volume stored CO_2 was not affected by the steeper anticline structure. If the geometry and especially the caprock had been even more different, the effect of if may affect the form of the CO_2 plume. CO_2 have lower density than water, and will ideally stay on top of the underlying water layer. Since the case is cyclic storage, with dynamic variation in pressure during each year, the form of the CO_2 plume will be affected dynamically with the pressures. If the case was just storage without production of CO_2, the pressures would affect the form of the CO_2 plume most in the beginning. With time, the plume would get more in equilibrium with the water and may look more like the situation in figure 2.1 from the review section. Note that the difference between the bottom hole pressure and the initial pressure in the reservoir helps to determine the amount of injected CO_2. Higher difference in this pressure therefore helps to drive the gas further out in the aquifer, leading to more trapped CO_2 because of bigger contact area at the gas-water contact. As shown above in figure 6.28, the effect of dissolution is important. More CO_2 will increasingly dissolve in water with time. Figure 6.31 shows more in detail why there is CO_2 loss in the system. It shows the increasing loss after one and two cycles, and that CO_2 dissolves more in the upper layer at the gas-water contact with time. As mentioned in the section for residual trapping, some water is probably produced, and may lead to less produced CO_2.

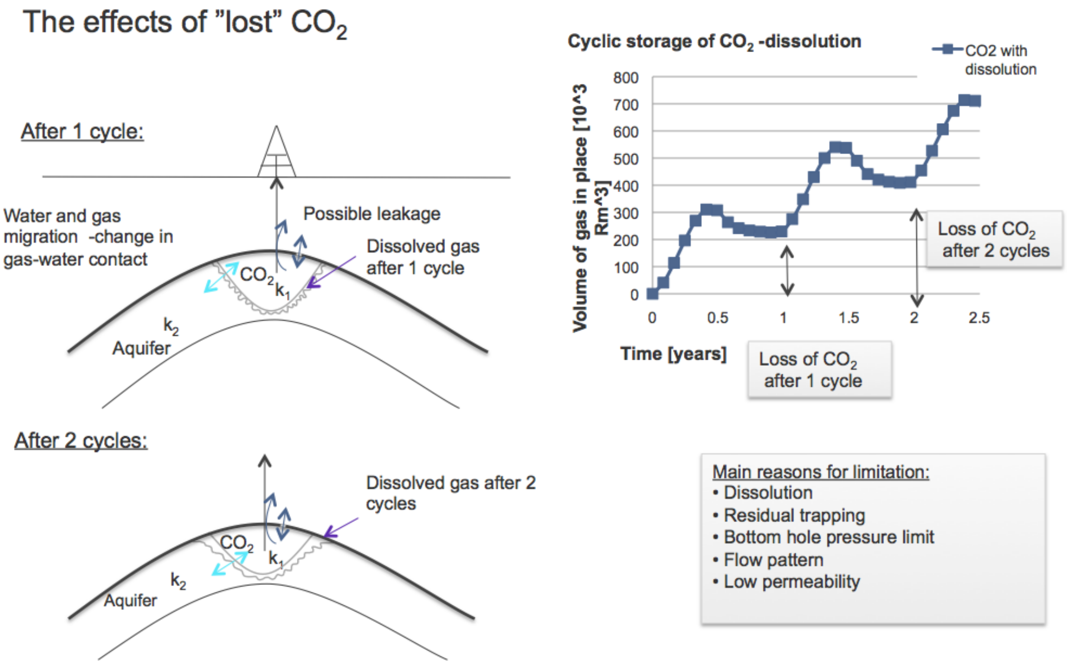
The effects of "lost" CO2
After 1 cycle:
Water and gas migration -change in gas-water contact
Possible leakage
Dissolved gas after 1 cycle
CO2
k1
k2
Aquifer
After 2 cycles:
Dissolved gas after 2 cycles
CO2
k1
k2
Aquifer
Cyclic storage of CO2 -dissolution
CO2 with dissolution
Volume of gas in place [10^3 Rm^3]
800
700
600
500
400
300
200
100
0
0
0.5
1
1.5
2
2.5
Time [years]
Loss of CO2 after 1 cycle
Loss of CO2 after 2 cycles
Main reasons for limitation:
• Dissolution
• Residual trapping
• Bottom hole pressure limit
• Flow pattern
• Low permeability

FIGURE 6.31: Residual saturation of CO_2 after 4 years of cyclic storage for a realistic case, versus an ideal case.

How big the area of the gas-water contact is, is essential. In this case, the geology is homogenous, and the gas-water contact area is symmetrical around the well. Together with the effects of aquifer support, the bottom hole pressure support, and residual trapping during cyclic storage of CO_2, the dissolved CO_2 tends to increase with time, and especially along the caprock. Main effects for limitations of CO_2 production are summarized in figure 6.31 .

Weakness of simulation of dissolution is present. Dissolution effects in a geology like in this model may be a bit tricky. Several cases should be done to get more reliable results, because the grid block size in the model may cause the big effect of dissolution, instead of the physics.

6.4 Summary of the application of the model in Eclipse

In the five previous sections, sensitivity of different parameters has been done. A summary of the most important observations is shown in table 6.2.

Table 6.2: The different simulation cases and their most important observations.

Simulation Cases	
Sensitivity of parameters	**Observations**
Permeability:	When permeability decrease, higher pressure is needed both for methane and CO_2.
Aquifer pressure support:	When the aquifer pressure decrease less methane is stored, while CO_2 sligthly decrease the amount stored.
Geometry:	A steeper anticline structure did not affect CO_2. The volume of methane slightly increased.
Dissolution:	With time, more and more CO_2 dissolve in water.
Residual trapping:	Both methane and CO_2 increase residual trapping with hysteresis

From the observations, both CO_2 and methane respond similar to several of the cases, but there are also seen significant differences between the gases. The main differences is that CO_2 is less compressible than methane, and that CO_2 dissolve in water which methane does not, and the difference in density behaviour where CO_2 varies greatly by the pressure. Because of differences, and based on the simulation study, a bigger loss of CO_2 will take place during cyclic storage. In order to implement cyclic storage of CO_2, the volume of trapped gas term in the model (see equation 3.3) should be extracted and focused on.

7. Discussion

Seasonal storage of dry methane gas is a well-established technique, but can it work for CO_2? Parameters which appear to be important in cyclic storage of CO_2 are the effect of dissolved CO_2 in water, residual trapping, and the flow pattern of CO_2 which is affected by the aquifer pressure support, permeability in the aquifer, and the value of the injection and production pressure. Figure 7.1 shows the important parameters.

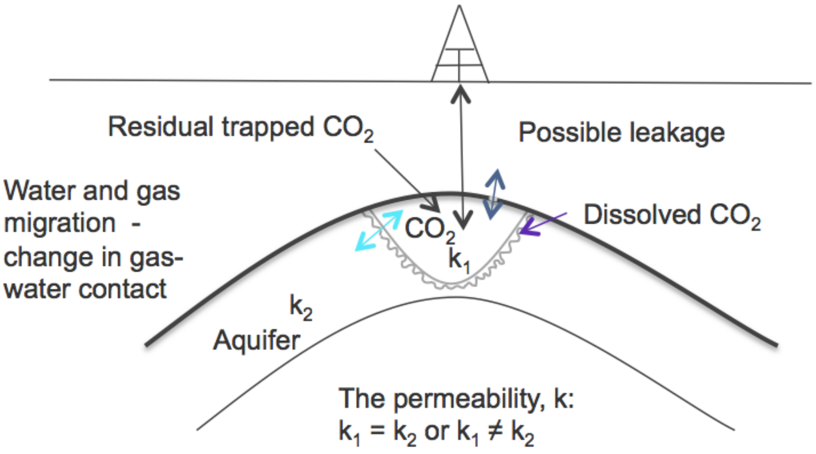
Residual trapped CO₂
Possible leakage
Water and gas migration - change in gas-water contact
CO₂
k₁
Dissolved CO₂
k₂
Aquifer
The permeability, k:
k₁ = k₂ or k₁ ≠ k₂

FIGURE 7.1: Cyclic storage of CO_2 showing important factors.

Comparison Between the Sensitivity Analysis and the Eclipse Model: A model for modelling natural gas reservoirs has been tested and validated. Sensitivity analysis of parameters in the implicit method has been performed. It was questioned whether the Collier model was correct or not. However, the approximate model in Eclipse functioned well.

The observations worth noting from the sensitivity analysis of the implicit method are:

- The water drive constant (C^*)

- The gas entrapment factor (F_g)
- The initial amount of gas in place (G_i).

While moving from the implicit method to the Eclipse model, a change from analysing cyclic storage of methane in a 0-dimentional model, to analyse the gases in a 3-dimentional model was done. The 3-dimentional model was an homogenous model dependent on transport properties. The simulated model in Eclipse was a good match considering these factors. The importance of the water drive constant (C^*) corresponds to the pressure support ($\dot{W}_e$) from the aquifer, which was an important observation in both the models. The relation is seen in equation 3.2. The importance of the gas entrapment factor corresponds to the effect of dissolution and residual trapping in the 3-dimentional simulated model, which are essential for cyclic storage of CO_2 versus methane.

The Effect of Compressibility and Density:

Based on figure 6.7, CO_2 is less compressible than methane. All the cases had higher-pressure variations than methane, and needed higher average pressures in order to store and inject enough. The pressure in the fluid column is different for methane and CO$_2$, where the weight of CO_2 column will weigh more than methane. This observation is interesting when it comes to comparing how large pressures that is needed during cyclic storage of both the gases. CO_2 differ from methane by being stored as a supercritical fluid where the density highly vary with the function of pressure. However, methane injected into water gives lower viscosity in the reservoir and will lead to easier production.

The Effect of Lost CO_2:

Residual trapped gas will occur during storage both for methane and CO_2. The ideal average pressure function for injection and production of gas, inject and produce the same amount of gas with a low percent of gas loss. In reality, based on the simulations, both methane and CO_2 will have loss of gas to the formation. An important observation is that a higher value of injected CO_2 gets lost compared to methane. With time, more CO_2 will dissolved in water, which methane is assumed not to. Dissolved CO_2 in water cause denser water. Each year, more and more CO_2 will be trapped, and it appears to be a dynamical movement of the gas in the aquifer. Since the volume of gas will vary in the reservoir, a fraction of water will be produced during production. The contact area of gas-water together with time is essential for how large the value of dissolved CO_2 will be. Figure 6.31 in the section for dissolution, showed that a reservoir may have a different permeability than an aquifer, which will affect the aquifer pressure support. It also tells that the injection and production pressure from the well affects the flow pattern of CO_2. Migration of CO_2 leads to larger contact area with time, and therefore a larger amount of trapped and dissolved CO_2. Figure 7.2 shows the effect of simulated cyclic storage of CO_2 versus a generalized ideal storage case with a minimal loss of gas. It shows that a realistic value of lost CO_2 may be 73%.

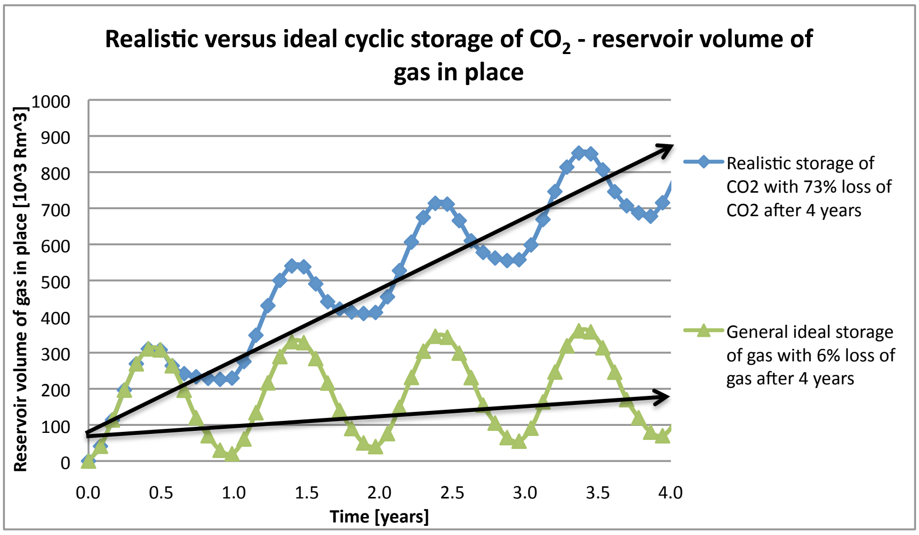

FIGURE 7.2: Residual saturation of CO_2 after 4 years of cyclic storage for a realistic case, versus an ideal case.

Further Work:

This study shows that cyclic storage of CO_2 is possible. If the concept is going to be implemented in real life, the model for modelling natural gas storage, tested and validated in the earlier chapters, should be revised for modelling CO_2 storage. In order to implement cyclic storage of CO_2, volume of the trapped gas term in the model (equation 3.3), should be extracted and focused on. On a large scale, CO_2 emissions might be reduced, while used in EOR projects, which might prevent global temperature rise.

8. Conclusion

To create value for CO_2 storage, and make it economic, temporary storage of CO_2 for the purpose to be used in EOR projects, might be a solution.

CO_2 may not be stored exactly in the same way as methane, but they are comparable in many ways. CO_2 cyclic storage has a bigger loss in CO_2 for each cycle, and needs a higher pressure in order to re-produce enough CO_2 compared to methane.

The important parameters for cyclic storage of CO_2 are the effect of dissolved CO_2 in water, residual trapping, and the flow pattern of CO_2 which is affected by the aquifer pressure support, permeability in the aquifer, and the value og the injection and production pressures.

If CO_2 is going to be stored temporarily, the model for modelling natural gas storage tested and validated in earlier chapters, should be revised for modelling CO_2 storage with a focus on ”lost” CO_2.

A. Calculations of the Gas-Water Contact

To find the gas-water contact, a method using the volume of a rotational body with a cylindrical coordinate system is used.

Given

$$H = aR_m^2 \tag{A.1}$$

$$a = \frac{H}{R_m^2} \tag{A.2}$$

where H denotes the hight of the anticline, h denote the depth from the cap rock to the phase contact, R_m denotes the radius of the anticline form, and a denotes the steepness of the anticline. See figures A.1 and A.2.

Derivation of the volume equation:

$$V(h) = \int_0^{2\pi} \int_0^{\sqrt{\frac{h}{a}}} \int_{ar^2}^{h} dx \cdot r \cdot dr \cdot d\theta \tag{A.3}$$

$$= 2\pi \int_0^{\sqrt{\frac{h}{a}}} (h - ar^2) r \cdot d\theta r \tag{A.4}$$

$$= 2\pi \left[\frac{1}{2} hr^2 - \frac{1}{4} ar^4 \right]_0^{\sqrt{\frac{h}{a}}} \tag{A.5}$$

$$= 2\pi \frac{1}{4} \cdot \frac{h^2}{a} = \frac{\pi h^2}{2a} = V(h) \tag{A.6}$$

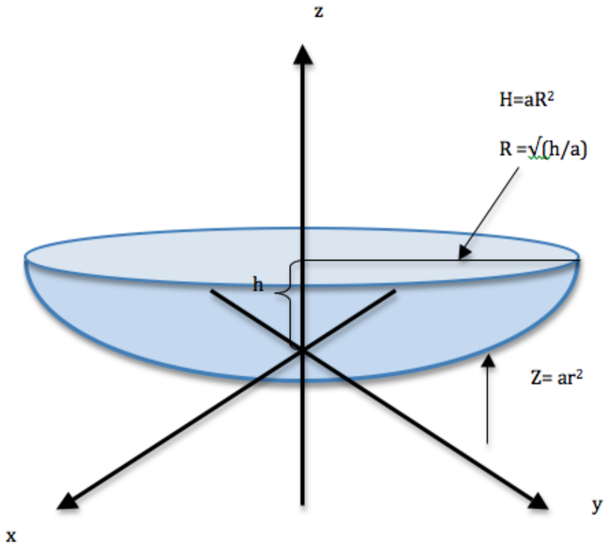

Figure A.1: Derivations of a gas volume using a rotational body with cylindrical coordinate system.

The volume equation is then:

$$V(h) = \frac{\pi h^2}{2 \cdot \frac{H}{R_m^2}} = \left(\frac{\pi R_m^2}{2H} \right) h^2 \tag{A.7}$$

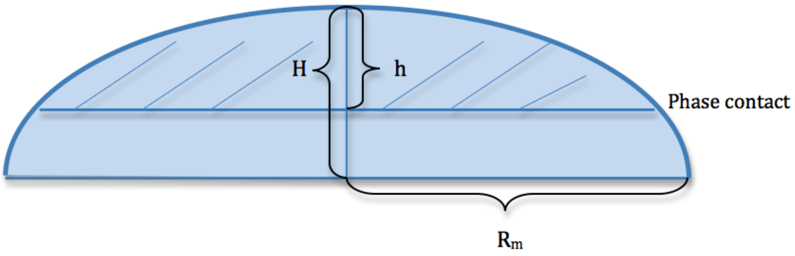

Figure A.2: Derivations of the depth from the cap rock down to the gas-water contact.

Desolve equation A.7 with respect to h:

$$h = \sqrt{\frac{2HV_{ginit}}{\pi R_m^2 \varphi (1 - S_{wi})}} < \quad H \tag{A.8}$$

where V_{ginit} denotes the given reservoir volume, φ denotes the reservoir porosity, and S_{wi} denotes the initial water saturation.

B. Data File for Cyclic Storage of Methane

```
RUNSPEC
'final2'

TITLE

DIMENS 75 75 10 \

OIL
GAS


SATOPTS
HYSTER \

UNIFIN
UNIFOUT


METRIC

NONNC

WELLDIMS
−− Well Dimension Data
−− NWMAXZ NCWMAX NGMAXZ NWGMAX
− − − − − − − − − − − − − − − − − − − − − − − − −−
10 10 2 10 \
−− NWMAXZ: Max. number of wells in the models.
−− NCWMAX: Max. number of conncections per well (i.e.. no. of perforations).
−− NGMAXZ: Max. nunmer of groups in the model.
−− NWGMAX: Max. number of wells in any one group
```

```
TABDIMS
−− Table Of Dimensions
−− NTSFUN NTPVT NSSFUN NPPVT NTFIP NRPVT
− − − − − − − − − − − − − − − − − − − − − − − − − − − − − − − − − −
2 1 8 20 1 20 \
−−NTSFUN: No. of saturation tables entered.
−− NTPVT : No. of PVT tables entered (in the PROPS section).
−− NSSFUN: Max. no. of saturation nodes in each saturation table
−− NPPVT : Max. number of pressure nodes in any pVT table
−− NTFIP : Max. number of FIP regions defined using FIPNUM
−− NRPVT : Max. number of Rs nodes in a live oil pVT table


START
1 JAN 2010 \

NSTACK
800 \

GRID ==================================

DX
56250*20.84 \


DY
56250*20.84 \


DZ
56250*10.0 \


INIT


BOX
1 75 1 75 1 1 \

INCLUDE
’../Metan/TOPSCO2.INC’ \
ENDBOX

PORO
56250*0.3 \

PERMX
56250*500 \

COPY
PERMX PERMY \
PERMX PERMZ \
\


PROPS =====================================

−− Use Killough’s model where oil is wetting, gas non-wetting

EHYSTR
0.1 7 \


DENSITY
−−surface conditions (temp 20C)
−− OIL WATER GAS
1000 0.0000 0.668
−−Bruker oil=water and gas=methane gas..
\


ROCK
−− Rock Compressibility −− Ref. pressure Compressibility − − − − − − − −
− − − − − − − − − − − − − − − − − − − − − −− 100 5.4e-5 \


PVDO
−− PVT data for temp =32C, and salinity = 4%

−−Pressure Bo Viscosity
−−bar Rm3/Sm3 mPa s
25 1.000 0.85
```

```
50 0.995 0.85
75 0.990 0.85
100 0.985 0.85
125 0.980 0.85
150 0.975 0.85
175 0.970 0.85 \


PVDG
−−stdcond = 1bar,15C
−− res condition = 32C (fÂŕr T=35C) (approx. 1000 m below sea floor where temp = 4C)
−−Pressure Bg Visosity
−−bar rm3/Sm3 mPa s
50 0.019628615 0.014920503
60 0.01611849 0.01595846
70 0.013622349 0.017152346
80 0.011761481 0.018520424
90 0.010325525 0.020084482
100 0.009188238 0.021869977
110 0.008269205 0.02390627
120 0.007514685 0.026226923
130 0.006887316 0.02887003
140 0.006360231 0.031878553
150 0.005913546 0.035300669
160 0.005532173 0.0391901
170 0.005204423 0.043606438
180 0.004921073 0.048615438
190 0.004674743 0.054289292
200 0.00445946 0.060706875
210 0.004270343 0.06795397
220 0.004103377 0.07612347
230 0.003955245 0.085315471
240 0.003823191 0.095637706
250 0.003704921 0.107205399
\
SOF2
−− So Krog
0.25 0
0.375 0.002777778
0.5 0.022222222
0.625 0.075
0.75 0.177777778
0.875 0.347222222
1 0.6 \

0.25 0
0.308333333 0.011111111
0.366666667 0.044444444
0.425 0.1
0.483333333 0.177777778
0.541666667 0.277777778
0.6 0.4 \

SGFN
−− Sg Krg pcog
0 0 0
0.125 0.003703704 0.000457764
0.25 0.02962963 0.014648438
0.375 0.1 0.111236572
0.5 0.237037037 0.46875
0.625 0.462962963 1.430511475
0.75 0.8 3.559570313 \

0.4 0 0
0.458333333 0.003703704 0.002746862
0.516666667 0.02962963 0.043949786
0.575 0.1 0.222495793
0.633333333 0.237037037 0.70319658
0.691666667 0.462962963 1.716788526
```

```
0.75 0.8 3.559570313 \


REGIONS ===============================================


SATNUM
56250*1 \


IMBNUM 56250*2 \


SOLUTION ============================================

EQUIL
−−datum Pinit woc pcow goc pcgo rs rv accuracy
1000 100 1900.0 0.0 700 0.0 \


RPTRST
BASIC=2 \
−− BASIC=2 means that restart files are written at every report time step


RPTSOL
FIP=1 PRESSURE SGAS RS RESTART=1 \


SUMMARY ===========================================
− − −THIS SECTION SPECIFIES DATA TO BE WRITTEN TO THE SUM-
MARY FILES
− − −AND WHICH MAY LATER BE USED WITH THE ECLIPSE GRAPHICS
PACKAGE
− − − − − − − − − − − − − − − − − − − − − − − − − − − − − − − − − − − − −
− − − − − − − − − − − − − − − − − − − − − − − − − − − − −
FPR
FGIPG
FGIPL
FGIT
```

```
FGDEN
FGIPR
FVIT
FGPTF
FGPTS
FVIR
FVPT
FGPT
FOPT
FOPR
WBHP
\
SEPARATE
RPTONLY
RUNSUM
EXCEL


SCHEDULE==================================
− − − − − −−THIS SECTION SPECIFIES THE OPERATIONS TO BE SIMULATED
− − − − − − − − − − − − − − − − − − − − − − − − − − − − − − − − − − − −
− − − − − − − − − − − − − − − − −−


MESSAGES
−− Print limits Stop limits
−− Messages Comments Warning Problems Error Bug Messages Comments Warnings Problems Error Bug
6000 6000 10000 100000 2 100 60000 60000 100000 1000000 2 100 \


WELSPECS
−− General Spesification Data For Wells
−− WELL WELL L O C A T I O N BHP PREF.
−− NAME GROUP I J DATUM PHASE
− − − − − − − − − − − − − − − − − − − − − − − − − − − − − − − − −
'G1' 'INJ' 37 37 1* 'GAS' \
'W1' 'PRO' 37 37 1* 'GAS' \
\


COMPDAT
−− Connection Between Wells and Blocks
−− WELL L O C A T I O N Saturation Transmis. Well Bore
−− NAME I J K(upper) K(lower) STATUS Table No. Factor Diameter Eff. Kh Skin D-fact Direction
− − − − − − − − − − − − − − − − − − − − − − − −
'G1' 37 37 1 1 'OPEN' 0 1* 0.1 1* 1* 1* X \
'W1' 37 37 1 1 'OPEN' 0 1* 0.1 1* 1* 1* X \
\


−−NEWRATEFUNCTION : R(T) = 0,02831∗1e6∗365∗50∗SIN(DT∗2PI)


WCONINJ
−− Control Data For Injection Wells
−− WELL INJ CONTROL FLOW-RATE-TARGET REINJECTION BHP THP VFP VAPORIZED OIL IN
−− NAME TYPE STATUS MODE SURFACE RESERVOIR FRACTION FLAG TARGET TARGET TABLE# INJECTION GAS
−−−−−−−−−−−−−−−−−−−−−−−−−−−−−−−−−−−−−−−−−−−−
'G1' 'GAS' 'OPEN' 'RESV' 1* 1780 1* 'NONE' 300 1* 1* 1* \
\


WCONPROD
−− Control Data For Production Wells
−− WELL OPEN/SHUT CONTROL SURFAC-RATE-TARGET REINJECTION BHP THP VFP VAPORIZED OIL IN
−− NAME STATUS MODE OIL WAT GAS FRACTION FLAG TARGET TARGET TABLE# INJECTION GAS
'W1' 'SHUT' 'RESV' 1* 1* 1* 1* 1530 1 \
\
TSTEP
30 \

WCONINJ
−− Control Data For Injection Wells
−− WELL INJ CONTROL FLOW-RATE-TARGET REINJECTION BHP THP
VFP VAPORIZED OIL IN
−− NAME TYPE STATUS MODE SURFACE RESERVOIR FRACTION FLAG
TARGET TARGET TABLE# INJECTION GAS
−−−−−−−−−−−−−−−−−−−−−−−−−−−−−−−−−−−−−−−−−−−−
’G1’ ’GAS’ ’OPEN’ ’RESV’ 1* 3024 1* ’NONE’ 300 1* 1* 1* \
\

TSTEP
30 \

WCONINJ
−− Control Data For Injection Wells
−− WELL INJ CONTROL FLOW-RATE-TARGET REINJECTION BHP THP
VFP VAPORIZED OIL IN
−− NAME TYPE STATUS MODE SURFACE RESERVOIR FRACTION FLAG
TARGET TARGET TABLE# INJECTION GAS
−−−−−−−−−−−−−−−−−−−−−−−−−−−−−−−−−−−−−−−−−−−−
’G1’ ’GAS’ ’OPEN’ ’RESV’ 1* 3415 1* ’NONE’ 300 1* 1* 1* \
\

TSTEP
30 \

WCONINJ
−− Control Data For Injection Wells
−− WELL INJ CONTROL FLOW-RATE-TARGET REINJECTION BHP THP
VFP VAPORIZED OIL IN
−− NAME TYPE STATUS MODE SURFACE RESERVOIR FRACTION FLAG
```

```
TARGET TARGET TABLE# INJECTION GAS
−−−−−−−−−−−−−−−−−−−−−−−−−−−−−−−−−−−−−−−−−−
’G1’ ’GAS’ ’OPEN’ ’RESV’ 1* 2904 1* ’NONE’ 300 1* 1* 1* \
\

TSTEP
30 \

WCONINJ
−− Control Data For Injection Wells
−− WELL INJ CONTROL FLOW-RATE-TARGET REINJECTION BHP THP
VFP VAPORIZED OIL IN
−− NAME TYPE STATUS MODE SURFACE RESERVOIR FRACTION FLAG
TARGET TARGET TABLE# INJECTION GAS
−−−−−−−−−−−−−−−−−−−−−−−−−−−−−−−−−−−−−−−−−−
’G1’ ’GAS’ ’OPEN’ ’RESV’ 1* 1622 1* ’NONE’ 300 1* 1* 1* \
\

TSTEP
30 \

WCONINJ
−− Control Data For Injection Wells
−− WELL INJ CONTROL FLOW-RATE-TARGET REINJECTION BHP THP
VFP VAPORIZED OIL IN
−− NAME TYPE STATUS MODE SURFACE RESERVOIR FRACTION FLAG
TARGET TARGET TABLE# INJECTION GAS
−−−−−−−−−−−−−−−−−−−−−−−−−−−−−−−−−−−−−−−−−−
’G1’ ’GAS’ ’SHUT’ ’RESV’ 1* 1622 1* ’NONE’ 300 1* 1* 1* \
\

WCONPROD
−− Control Data For Production Wells
−− WELL OPEN/SHUT CONTROL SURFAC-RATE-TARGET REINJECTION
```

```
BHP THP VFP VAPORIZED OIL IN
−− NAME STATUS MODE OIL WAT GAS FRACTION FLAG TARGET TARGET TABLE# INJECTION GAS
’W1’ ’OPEN’ ’RESV’ 1* 1* 1* 1* 84 1 \
\

TSTEP
30 \

WCONPROD
−− Control Data For Production Wells
−− WELL OPEN/SHUT CONTROL SURFAC-RATE-TARGET REINJECTION
BHP THP VFP VAPORIZED OIL IN
−− NAME STATUS MODE OIL WAT GAS FRACTION FLAG TARGET TARGET TABLE# INJECTION GAS
’W1’ ’OPEN’ ’RESV’ 1* 1* 1* 1* 1738 1 \
\

TSTEP
30 \

WCONPROD
−− Control Data For Production Wells
−− WELL OPEN/SHUT CONTROL SURFAC-RATE-TARGET REINJECTION
BHP THP VFP VAPORIZED OIL IN
−− NAME STATUS MODE OIL WAT GAS FRACTION FLAG TARGET TARGET TABLE# INJECTION GAS
’W1’ ’OPEN’ ’RESV’ 1* 1* 1* 1* 2950 1 \
\

TSTEP
30 \
WCONPROD
−− Control Data For Production Wells
−− WELL OPEN/SHUT CONTROL SURFAC-RATE-TARGET REINJECTION
BHP THP VFP VAPORIZED OIL IN
−− NAME STATUS MODE OIL WAT GAS FRACTION FLAG TARGET TAR-
GET TABLE# INJECTION GAS
’W1’ ’OPEN’ ’RESV’ 1* 1* 1* 1* 3364 1 \
\


TSTEP
30 \


WCONPROD
−− Control Data For Production Wells
−− WELL OPEN/SHUT CONTROL SURFAC-RATE-TARGET REINJECTION
BHP THP VFP VAPORIZED OIL IN
−− NAME STATUS MODE OIL WAT GAS FRACTION FLAG TARGET TAR-
GET TABLE# INJECTION GAS
’W1’ ’OPEN’ ’RESV’ 1* 1* 1* 1* 2860 1 \
\


TSTEP
30 \


WCONPROD
−− Control Data For Production Wells
−− WELL OPEN/SHUT CONTROL SURFAC-RATE-TARGET REINJECTION
BHP THP VFP VAPORIZED OIL IN
−− NAME STATUS MODE OIL WAT GAS FRACTION FLAG TARGET TAR-
GET TABLE# INJECTION GAS
’W1’ ’OPEN’ ’RESV’ 1* 1* 1* 1* 1570 1 \
\
TSTEP
30 \


WCONPROD
−− Control Data For Production Wells
−− WELL OPEN/SHUT CONTROL SURFAC-RATE-TARGET REINJECTION BHP THP VFP VAPORIZED OIL IN
−− NAME STATUS MODE OIL WAT GAS FRACTION FLAG TARGET TARGET TABLE# INJECTION GAS
'W1' 'SHUT' 'RESV' 1* 1* 1* 1* 1570 1 \
\


WCONINJ
−− Control Data For Injection Wells
−− WELL INJ CONTROL FLOW-RATE-TARGET REINJECTION BHP THP VFP VAPORIZED OIL IN
−− NAME TYPE STATUS MODE SURFACE RESERVOIR FRACTION FLAG TARGET TARGET TABLE# INJECTION GAS
− − − − − − − − − − − − − − − − − − − − − − − − − − − − − − − − − − − − − − − − − − − − − − − − − − − −
'G1' 'GAS' 'OPEN' 'RESV' 1* 175 1* 'NONE' 300 1* 1* 1* \
\


TSTEP
30 \
− − −− One cycle finished
WTEST
−− Name Period Reason Maximum tests
− − − − − − − − − − − − − − − − − − − − − − − − − − − − −
'G1' 0.5 'P' 1* \
'W1' 0.5 'P' 1* \
\
END
```

C. Data File for Cyclic Storage of CO_2

```
RUNSPEC


TITLE
'final2'


DIMENS
75 75 10 \


OIL
GAS
DISGAS


SATOPTS
HYSTER \


UNIFIN
UNIFOUT


METRIC

NONNC

WELLDIMS
−− Well Dimension Data
−− NWMAXZ NCWMAX NGMAXZ NWGMAX
```

```
− − − − − − − − − − − − − − − − − − − − − − − − − − −− 10 10 2 10 \
−− NWMAXZ: Max. number of wells in the models.
−− NCWMAX: Max. number of conncections per well (i.e.. no. of perforations).
−− NGMAXZ: Max. nunmer of groups in the model.
−− NWGMAX: Max. number of wells in any one group


TABDIMS
−− Table Of Dimensions
−− NTSFUN NTPVT NSSFUN NPPVT NTFIP NRPVT
− − − − − − − − − − − − − − − − − − − − − − − − − − − − − − − − − − −−
2 1 8 20 1 20 \
−− NTSFUN: No. of saturation tables entered.
−− NTPVT : No. of PVT tables entered (in the PROPS section).
−− NSSFUN: Max. no. of saturation nodes in each saturation table
−− NPPVT : Max. number of pressure nodes in any pVT table
−− NTFIP : Max. number of FIP regions defined using FIPNUM
−− NRPVT : Max. number of Rs nodes in a live oil pVT table


START
1 JAN 2010 \


NSTACK
800 \


GRID =======================================

DX
56250*20.84 \


DY
56250*20.84 \
DZ
56250*10.0 \

INIT

BOX
1 75 1 75 1 1 \

INCLUDE
’../NYCO2/TOPSCO2.INC’ \

ENDBOX

PORO
56250*0.3 \

PERMX
56250*500 \

COPY
PERMX PERMY \
PERMX PERMZ \
\

PROPS ==========================================

−− Use Killough’s model where oil is wetting, gas non-wetting

EHYSTR
0.1 7 \
DENSITY
−− surface conditions (temp 20C,should be 15C)
−− OIL WATER GAS
1000 0.0000 1.85
−− Bruker oil=water and gas=CO2
\


ROCK
−− Rock Compressibility
−− Ref. pressure Compressibility − − − − − − − − − − − − − − − − − − − −
− − − − − − − − − −− 100 5.4e-5 \


PVTO
−− PVT data for temp = 35C, and salinity = 3

−− Rs Pressure Bo Viscosity
−−Sm3/m3 bar Rm3/Sm3 mPa s
0 1 1 0.758092508
20 0.999185073 0.758139999
50 0.99790782 0.758214984
100 0.995804402 0.758339959
150 0.993731942 0.758464934 \


5.88648778 10 1.00817151 0.75811500
30 1.00731418 0.75816499
70 1.005614919 0.75826497
150 1.002276495 0.75846493 \


15.83009052 30 1.021752662 0.7581649
60 1.02047145 0.7582399
100 1.018780946 0.7583399
150 1.016695801 0.7584649 \
23.377942 50 1.031842577 0.758214
80 1.030565433 0.758289
120 1.028880218 0.758389
150 1.027629312 0.758464 \

28.39734679 70 1.038261527 0.75826
100 1.036989645 0.75833
120 1.036147993 0.75838
150 1.034894789 0.75846 \

30.40603043 90 1.040320509 0.7583
120 1.039055237 0.758301
150 1.037801121 0.7584 \

31.16339167 110 1.040571842 0.758001
130 1.039731834 0.75801
150 1.03889676 0.7581 \
\

PVDG
−−stdcond = 1bar,15C
−− res condition = 32C (fÂŕr T=35C) (approx. 1000 m below sea floor where temp = 4C)
−−Pressure Bg Visosity
−−bar rm3/Sm3 mPa s
50 0.015404546 0.016831183
60 0.011284993 0.017936162
70 0.007745867 0.020496746
80 0.002870396 0.050174688
90 0.002613015 0.058098666
100 0.002495864 0.062851068
110 0.002418559 0.066537743
120 0.002360704 0.06965196
130 0.002314469 0.072398824
```

```
140 0.002275971 0.074886605
150 0.002242997 0.077180529
160 0.002214163 0.079323312
170 0.002188546 0.081344592
180 0.002165501 0.083265832
190 0.002144559 0.085103102
200 0.002125369 0.086868762
210 0.002107661 0.088572533
220 0.002091224 0.090222207
230 0.002075888 0.091824129
240 0.002061516 0.09338354
250 0.002047995 0.094904824\
\


SOF2
−− So Krog
0.25 0
0.375 0.002777778
0.5 0.022222222
0.625 0.075
0.75 0.177777778
0.875 0.347222222
1 0.6 \


0.25 0
0.308333333 0.011111111
0.366666667 0.044444444
0.425 0.1
0.483333333 0.177777778
0.541666667 0.277777778
0.6 0.4 \


SGFN
−− Sg Krg pcog
0 0 0
```

```
0.125 0.003703704 0.000457764
0.25 0.02962963 0.014648438
0.375 0.1 0.111236572
0.5 0.237037037 0.46875
0.625 0.462962963 1.430511475
0.75 0.8 3.559570313 \


0.4 0 0
0.458333333 0.003703704 0.002746862
0.516666667 0.02962963 0.043949786
0.575 0.1 0.222495793
0.633333333 0.237037037 0.70319658
0.691666667 0.462962963 1.716788526
0.75 0.8 3.559570313 \


REGIONS ============================================

SATNUM
56250*1 \


IMBNUM
56250*2 \


SOLUTION ========================================

EQUIL
−−datum Pinit woc pcow goc pcgo rs rv accuracy
1000 100 1900.0 0.0 700.0 0.0 1 0 \


RPTRST
BASIC=2 \
−− BASIC=2 means that restart files are written at every report time step
```

```
RPTSOL
FIP=1 PRESSURE SGAS RS RESTART=1 \


RSVD
−−Depth Rs
800 0.00000000
1350 0.00000000 \


SUMMARY =========================================
− − −THIS SECTION SPECIFIES DATA TO BE WRITTEN TO THE SUMMARY FILES
−−−AND WHICH MAY LATER BE USED WITH THE ECLIPSE GRAPHICS PACKAGE
− − − − − − − − − − − − − − − − − − − − − − − − − − − − − − − − − − −
− − − − − − − − − − − − − − − − − − − − − − − − − − −
FPR
FGIPG
FGIPL
FGIT
FGDEN
FGIPR
FVIT
FGPTF
FGPTS
FVIR
FVPT
FGPT
FOPT
FOPR
WBHP
\
SEPARATE
RPTONLY
RUNSUM
```

```
EXCEL


SCHEDULE====================================
− − − − −−THIS SECTION SPECIFIES THE OPERATIONS TO BE SIMULATED
− − − − − − − − − − − − − − − − − − − − − − − − − − − − − − − − − − − − − − − −
− − − − − − − − − − − − − − − − −−


MESSAGES
−− Print limits Stop limits
−− Messages Comments Warning Problems Error Bug Messages Comments Warnings Problems Error Bug
6000 6000 10000 100000 2 100 60000 60000 100000 1000000 2 100 \


WELSPECS
−− General Spesification Data For Wells
−− WELL WELL L O C A T I O N BHP PREF.
−− NAME GROUP I J DATUM PHASE
− − − − − − − − − − − − − − − − − − − − − − − − − − − − − − − − − − −
’G1’ ’INJ’ 37 37 1* ’GAS’ \
’W1’ ’PRO’ 37 37 1* ’GAS’ \
\


COMPDAT
−− Connection Between Wells and Blocks
−− WELL L O C A T I O N Saturation Transmis. Well Bore
−− NAME I J K(upper) K(lower) STATUS Table No. Factor Diameter Eff. Kh Skin D-fact Direction
− − − − − − − − − − − − − − − − − − − − − − −−
’G1’ 37 37 1 1 ’OPEN’ 0 1* 0.1 1* 1* 1* X \
’W1’ 37 37 1 1 ’OPEN’ 0 1* 0.1 1* 1* 1* X \
\
--NEWRATEFUNCTION : R(T) = 0,02831*1e6*365*50*SIN(DT*2PI)


WCONINJ
-- Control Data For Injection Wells
-- WELL INJ CONTROL FLOW-RATE-TARGET REINJECTION BHP THP VFP VAPORIZED OIL IN
-- NAME TYPE STATUS MODE SURFACE RESERVOIR FRACTION FLAG TARGET TARGET TABLE# INJECTION GAS
-------------------------------------------
’G1’ ’GAS’ ’OPEN’ ’RESV’ 1* 1780 1* ’NONE’ 300 1* 1* 1* \
\


WCONPROD
-- Control Data For Production Wells
-- WELL OPEN/SHUT CONTROL SURFAC-RATE-TARGET REINJECTION BHP THP VFP VAPORIZED OIL IN
-- NAME STATUS MODE OIL WAT GAS FRACTION FLAG TARGET TARGET TABLE# INJECTION GAS
’W1’ ’SHUT’ ’RESV’ 1* 1* 1* 1* 1530 1 \
\


TSTEP
30 \


WCONINJ
-- Control Data For Injection Wells
-- WELL INJ CONTROL FLOW-RATE-TARGET REINJECTION BHP THP VFP VAPORIZED OIL IN
-- NAME TYPE STATUS MODE SURFACE RESERVOIR FRACTION FLAG TARGET TARGET TABLE# INJECTION GAS
-------------------------------------------
’G1’ ’GAS’ ’OPEN’ ’RESV’ 1* 3024 1* ’NONE’ 300 1* 1* 1* \
\
TSTEP
30 \


WCONINJ
−− Control Data For Injection Wells
−− WELL INJ CONTROL FLOW-RATE-TARGET REINJECTION BHP THP
VFP VAPORIZED OIL IN
−− NAME TYPE STATUS MODE SURFACE RESERVOIR FRACTION FLAG
TARGET TARGET TABLE# INJECTION GAS
−−−−−−−−−−−−−−−−−−−−−−−−−−−−−−−−−−−−−−−−−−−−−−−
'G1' 'GAS' 'OPEN' 'RESV' 1* 3415 1* 'NONE' 300 1* 1* 1* \
\


TSTEP
30 \


WCONINJ
−− Control Data For Injection Wells
−− WELL INJ CONTROL FLOW-RATE-TARGET REINJECTION BHP THP
VFP VAPORIZED OIL IN
−− NAME TYPE STATUS MODE SURFACE RESERVOIR FRACTION FLAG
TARGET TARGET TABLE# INJECTION GAS
−−−−−−−−−−−−−−−−−−−−−−−−−−−−−−−−−−−−−−−−−−−−−−−
'G1' 'GAS' 'OPEN' 'RESV' 1* 2904 1* 'NONE' 300 1* 1* 1* \
\


TSTEP
30 \


WCONINJ
−− Control Data For Injection Wells
−− WELL INJ CONTROL FLOW-RATE-TARGET REINJECTION BHP THP
VFP VAPORIZED OIL IN
−− NAME TYPE STATUS MODE SURFACE RESERVOIR FRACTION FLAG
```

```
TARGET TARGET TABLE# INJECTION GAS
−−−−−−−−−−−−−−−−−−−−−−−−−−−−−−−−−−−−−−−−−−−
'G1' 'GAS' 'OPEN' 'RESV' 1* 1622 1* 'NONE' 300 1* 1* 1* \
\


TSTEP
30 \


WCONINJ
−− Control Data For Injection Wells
−− WELL INJ CONTROL FLOW-RATE-TARGET REINJECTION BHP THP
VFP VAPORIZED OIL IN
−− NAME TYPE STATUS MODE SURFACE RESERVOIR FRACTION FLAG
TARGET TARGET TABLE# INJECTION GAS
−−−−−−−−−−−−−−−−−−−−−−−−−−−−−−−−−−−−−−−−−−−
'G1' 'GAS' 'SHUT' 'RESV' 1* 1622 1* 'NONE' 300 1* 1* 1* \
\


WCONPROD
−− Control Data For Production Wells
−− WELL OPEN/SHUT CONTROL SURFAC-RATE-TARGET REINJECTION
BHP THP VFP VAPORIZED OIL IN
−− NAME STATUS MODE OIL WAT GAS FRACTION FLAG TARGET
TARGET TABLE# INJECTION GAS
'W1' 'OPEN' 'RESV' 1* 1* 1* 1* 84 1 \
\


TSTEP
30 \


WCONPROD
−− Control Data For Production Wells
−− WELL OPEN/SHUT CONTROL SURFAC-RATE-TARGET REINJECTION
BHP THP VFP VAPORIZED OIL IN
```

```
−− NAME STATUS MODE OIL WAT GAS FRACTION FLAG TARGET TARGET TABLE# INJECTION GAS
’W1’ ’OPEN’ ’RESV’ 1* 1* 1* 1* 1738 1 \
\


TSTEP
30 \


WCONPROD
−− Control Data For Production Wells
−− WELL OPEN/SHUT CONTROL SURFAC-RATE-TARGET REINJECTION BHP THP VFP VAPORIZED OIL IN
−− NAME STATUS MODE OIL WAT GAS FRACTION FLAG TARGET TARGET TABLE# INJECTION GAS
’W1’ ’OPEN’ ’RESV’ 1* 1* 1* 1* 2950 1 \
\


TSTEP
30 \


WCONPROD
−− Control Data For Production Wells
−− WELL OPEN/SHUT CONTROL SURFAC-RATE-TARGET REINJECTION BHP THP VFP VAPORIZED OIL IN
−− NAME STATUS MODE OIL WAT GAS FRACTION FLAG TARGET TARGET TABLE# INJECTION GAS
’W1’ ’OPEN’ ’RESV’ 1* 1* 1* 1* 3364 1 \
\


TSTEP
30 \
WCONPROD
−− Control Data For Production Wells
−− WELL OPEN/SHUT CONTROL SURFAC-RATE-TARGET REINJECTION
BHP THP VFP VAPORIZED OIL IN
−− NAME STATUS MODE OIL WAT GAS FRACTION FLAG TARGET TAR-
GET TABLE# INJECTION GAS
’W1’ ’OPEN’ ’RESV’ 1* 1* 1* 1* 2860 1 \
\

TSTEP
30 \

WCONPROD
−− Control Data For Production Wells
−− WELL OPEN/SHUT CONTROL SURFAC-RATE-TARGET REINJECTION
BHP THP VFP VAPORIZED OIL IN
−− NAME STATUS MODE OIL WAT GAS FRACTION FLAG TARGET TAR-
GET TABLE# INJECTION GAS
’W1’ ’OPEN’ ’RESV’ 1* 1* 1* 1* 1570 1 \
\

TSTEP
30 \

WCONPROD
−− Control Data For Production Wells
−− WELL OPEN/SHUT CONTROL SURFAC-RATE-TARGET REINJECTION
BHP THP VFP VAPORIZED OIL IN
−− NAME STATUS MODE OIL WAT GAS FRACTION FLAG TARGET TAR-
GET TABLE# INJECTION GAS
’W1’ ’SHUT’ ’RESV’ 1* 1* 1* 1* 1570 1 \
\
WCONINJ
−− Control Data For Injection Wells
−− WELL INJ CONTROL FLOW-RATE-TARGET REINJECTION BHP THP
VFP VAPORIZED OIL IN
−− NAME TYPE STATUS MODE SURFACE RESERVOIR FRACTION FLAG
TARGET TARGET TABLE# INJECTION GAS
− − − − − − − − − − − − − − − − − − − − − − − − − − − − − − − − − − − − − − −
− − − − − − − − − − − − − − − − −
'G1' 'GAS' 'OPEN' 'RESV' 1* 175 1* 'NONE' 300 1* 1* 1* \
\


TSTEP
30 \
− − −− One cycle finished
WTEST
−− Name Period Reason Maximum tests
− − − − − − − − − − − − − − − − − − − − − − − − − − − − − − − − − −
'G1' 0.5 'P' 1* \
'W1' 0.5 'P' 1* \
\
END
```

Bibliography

R. Stuart Haszeldine. Carbon capture and storage: How green can black be? *Science*, 325:1647–1652, September 2009.

Niels E. Poulsen. The need for a co2 geological storage european atlas. *Energ Position Paper*, 2012.

Ola Eiken, Philip Ringrose, Christian Hermanrud, Bamshad Nazarian, Tore A. Torp, and Lars Høier. Lesson learned from 14 years of ccs operations: Sleipner, in salah and snøhvit. *Science Direct*, 2010.

Donald L. Katz and M. R. Tek. Overview on underground storage of natural gas. *Society of Petroleum Engineers*, 1981.

Richard S. Collier, ellis A. Monash, and Paul F. Hultquist. Modeling natural gas reservoirs -a simple model. *SPE*, 1981.

eia. The basics of underground natural gas storage.

R.F. Bietz, D.B. Bennion, and J. Patterson. Gas storage reservoir performance optimization through the application of drainage and imbibition relative permeability data. *The Journal of Canadian Petroleum Technology*, 35(2), 1996.

A.F. Van Everdingen and W. Hurst. The application of the laplace transformation to flow problems in reservoirs. *Journal of Petroleum Technology*, 1(12):305–324, december 1949.

J.F. Mayfield. Inventory verification of gas storage fields. *Society of Petroleum Engineers*, 1981.

Donald L. Katz, M. Rasin Tek, Keith H. Coats, Marvin L. Katz, Stanley C. Jones, and Maurice C. Miller. Movement of underground water in contact with natural gas, February 1963.

John W. Duane and Jackson Mich. Gas storage field development optimization. *Society of Petroleum Engineers*, October 1967.

D.L. Katz and D.P. Shah. Establishing the effective aquifer pressure controlling water drive for gas storage cycles. *SPE*, September 1984.